OPEN ACCESS

Scholars International Journal of Chemistry and Material Sciences

Abbreviated Key Title: Sch Int J Chem Mater Sci
ISSN 2616-8669 (Print) |ISSN 2617-6556 (Online)
Scholars Middle East Publishers, Dubai, United Arab Emirates
Journal homepage: http://saudijournals.com

Review Article

A Cross-Scale Design Grammar for Functional Matter: Integrating Synthetic Pathways, Reaction Mechanisms, Self-Assembly, Interfaces, Defect Chemistry, Multimodal Characterization, Predictive Modeling, and Performance Validation

Intazar Hussain Shah[1], Iqra Anjum[2], Laiba Javed[2], Waqar Yousaf[3], Irsa Liaqat4, Muhammad Yousaf Khan[5], Laiba Attique[6], Waheed Zaman Khan[7,8]*

[1]Centre of Excellence in Solid State Physics, University of the Punjab, Lahore, Pakistan
[2]International Islamic University Islamabad, H-10, Islamabad 44000, Pakistan
[3]Rosenheim University of Applied Sciences, Burghausen Campus, 84489 Burghausen, Germany
[4]Government College Women University Faisalabad, Faisalabad, Punjab, Pakistan
[5]University of Education, College Road, Township, Lahore 54770, Pakistan
[6]Government College University Faisalabad, Faisalabad, Punjab, Pakistan
[7]Department of Physics, Division of Science and Technology, University of Education, College Road, Township, Lahore 54770, Pakistan
[8]Moscow Institute of Physics and Technology, Phystech School of Aerospace Technology, 9 Institutskiy per., Dolgoprudny 141700, Russia

DOI: https://doi.org/10.36348/sijcms.2026.v09i02.002 | **Received:** 09.12.2025 | **Accepted:** 06.02.2026 | **Published:** 19.03.2026

***Corresponding author:** Waheed Zaman Khan
Department of Physics, Division of Science and Technology, University of Education, College Road, Township, Lahore 54770, Pakistan
Moscow Institute of Physics and Technology, Phystech School of Aerospace Technology, 9 Institutskiy per., Dolgoprudny 141700, Russia

Abstract

Functional matter is often designed and reported as disconnected advances in synthesis, structure, and performance, which limits transferability across materials classes and length scales. This review introduces a cross-scale design grammar that unifies how researchers specify, test, and validate causal links from processing and reactions to architecture, interfaces, defects, and device-level outcomes. We formalize grammar units as controllable operators, interaction rules, constraints, and measurable metrics, and show how uncertainty and failure modes propagate along the synthesis to structure to function chain. The framework integrates mechanistic control across solution, solid-state, vapor, electrochemical, and mechanochemical routes; mesoscale assembly and hierarchical architectures; interfaces and interphases as transport gatekeepers; and defect chemistry as both a performance lever and a degradation driver. We then treat multimodal characterization as an inference and evidence-fusion problem and map it onto a modeling ladder that spans mechanistic, continuum, statistical, and hybrid approaches with uncertainty quantification and validation. Finally, we provide benchmarking and reporting templates, truth-table criteria for what counts as improvement, and case-study scorecards that identify the dominant bottlenecks in representative applications. By converting fragmented knowledge into a reusable grammar, this review offers a practical, end-to-end playbook for designing functional matter with measurable causality, reproducibility, and observation-ready.

Keywords: Cross-Scale Design Grammar, Structure–Processing–Property–Performance, Interfaces and Interphases, Defect Chemistry and Degradation, Multimodal Characterization, Evidence Fusion, Uncertainty Quantification and Validation, Benchmarking and Reproducibility.

1. INTRODUCTION AND SCOPE

Functional matter is rarely limited by a single bottleneck. In real systems, performance emerges from coupled decisions that span precursors and processing history, reaction pathways and phase evolution, self-assembly and mesoscale architecture, interfacial chemistry and transport, defect populations and their

kinetics, measurement artifacts, model form uncertainty, and finally the credibility of benchmarking and validation. The central challenge is that these elements are typically studied in isolation, so the literature becomes a set of scale-specific optimizations rather than a transferable design logic. This fragmentation is not only conceptual, it is structural: even when high-quality mechanistic insights exist, they are scattered across papers, modalities, and communities and are often difficult to translate into actionable "if I change X, Y will happen, and Z will improve under these conditions" rules.

A useful historical lens is the process–structure–property–performance chain and the push toward integrated workflows. Integrated Computational Materials Engineering defined the goal explicitly as integrating materials information captured in computational tools with engineering performance analysis and manufacturing-process simulation, with the aim of turning materials into "design solutions" rather than selections from a static palette (National Research Council, 2008). The Materials Genome Initiative framed the same gap from a national innovation standpoint, emphasizing that incorporating new classes of materials into applications is typically about 10 to 20 years from initial research to first use, and arguing that acceleration demands coordinated infrastructure across computation, experiments, and data standards (OSTP, 2011).

The need for an explicit cross-scale grammar has intensified because modern tools can now generate and analyze data faster than we can establish causality. Self-driving laboratories and autonomous experimentation seek to operationalize a closed-loop scientific method through automated synthesis, measurement, and algorithmic experiment selection, and comprehensive reviews highlight rapid progress across chemistry and materials science (Tom *et al*., 2024; Tobias *et al*., 2025). However, fast loops amplify weak assumptions. Without a formal mapping between controllable operators, structural descriptors, and validated metrics, closed-loop systems can optimize confounded proxies, such as apparent improvements driven by testing artifacts, uncontrolled environment shifts, or subtle differences in contact geometry rather than intrinsic material changes.

At the same time, the community is beginning to make the fragmentation measurable. Large-scale efforts to extract mechanism statements from the literature argue that causal knowledge linking processing, structure, properties, and performance is dispersed and difficult to systematize, and they report mechanistic corpora at the scale of hundreds of thousands of extracted mechanisms supported by multimodal evidence (Liu *et al*., 2026). Complementary efforts have built autonomously generated materials knowledge graphs that cover the traditional processing-structure-property paradigm at scale, reporting over 70,000 entities and 5.4 million unique triples, which signals a shift toward machine-actionable structure that a design grammar can exploit (Venugopal *et al*., 2024). These developments support a practical conclusion: the bottleneck is moving from data scarcity to inference quality and validation discipline.

This review therefore proposes a cross-scale design grammar for functional matter. "Grammar" is used deliberately. A grammar is a finite set of primitives and rules that allows composition of many meaningful statements while also defining what counts as well formed. In materials terms, the primitives are: (i) control operators (synthesis and processing knobs), (ii) descriptors (quantified structure, interfaces, defects, architecture), (iii) constraints (thermodynamics, kinetics, manufacturability, safety, cost), (iv) metrics (property and performance measures with specified test conditions), and (v) validation rules (evidence thresholds, uncertainty handling, and benchmarking protocols). This framing aligns with the broader push for data stewardship and interoperability, where the FAIR guiding principles explicitly emphasize machine-actionable reuse as a prerequisite for robust, scalable science (Wilkinson *et al*., 2016).

A central theme throughout the review is that cross-scale linking must be causal, not just correlational. Correlation-driven optimization is fragile under distribution shift, for example changes in synthesis batch, humidity, electrode geometry, surface contamination, or measurement calibration. Recent work in reaction and process-structure-property contexts argues that causal inference can extract actionable cause-effect relationships and make findings more transferable than conventional black-box correlations, especially when interventions are explicit (Ting *et al*., 2022). In parallel, uncertainty quantification has become a practical necessity for predictive modeling in materials, because error bars often determine whether a predicted "improvement" is real or within noise. A benchmark-oriented review of uncertainty quantification methods for materials property prediction discusses concrete UQ techniques and emphasizes calibration and reliability rather than point accuracy alone (Varivoda *et al*., 2023).

The scope of the grammar is intentionally end-to-end. It begins with synthetic pathways and reaction mechanisms because these define what structural states are reachable and at what cost in defects and disorder. It then moves to self-assembly, hierarchical order, and mesoscale architecture because architecture often dominates functional outcomes via percolation, tortuosity, confinement, and interface density. It treats interfaces and interphases as function gatekeepers because many performance limits are interfacial and because interfaces are where artifacts hide. It treats defect chemistry as both a lever and a liability because defect populations can enable transport and activity while also accelerating degradation. It treats multimodal

characterization as an inference problem because no single technique provides a complete picture and because each modality has a sampling depth, damage mode, and artifact profile. For instance, X-ray photoelectron spectroscopy is frequently discussed as probing the near-surface, with a commonly cited information depth on the order of 10 nm for about 95 percent of detected signal under typical assumptions (Stevie, 2020). Time-of-flight secondary ion mass spectrometry is even more surface-sensitive, typically sampling only the upper 1 to 2 nm, so trace contamination or adventitious layers can dominate spectra and mislead mechanistic claims (Graham *et al*., 2023). Atomic force microscopy demonstrated vertical resolution below 1 angstrom in early reports, illustrating how measurement capability can exceed interpretability if surface state and environment are not controlled (Binnig *et al*., 1986). These numeric anchors are not trivia. They define what "surface," "interface," and "structure" mean operationally, and they determine what claims are logically supported.

This review does not aim to be a textbook of every synthesis route, a manual for every characterization technique, or a catalog of every model class. Instead, it provides a practical grammar that lets a reader convert a target function into a defensible plan: what knobs to vary, what descriptors to measure, what uncertainties to quantify, what failure modes to anticipate, and what validation criteria to satisfy before claiming improvement. The intended outcome is to help students and researchers produce work that is simultaneously mechanistically grounded, quantitatively reported, and portable across labs and platforms, including high-throughput and autonomous settings.

Students can use the review as a workflow template. Start from a target metric and explicitly define baselines and constraints. Choose control operators that plausibly intervene on causal mediators rather than superficial proxies. Design characterization as evidence fusion, where each claim is supported by at least two complementary modalities with different artifact profiles. Use modeling as a ladder, selecting the simplest level that can be validated against measurable descriptors and carrying uncertainty into decisions. Close the loop only when validation gates are met. This is the spirit of "design grammar": not more information, but better structured reasoning that survives scale-up, transfer, and replication.

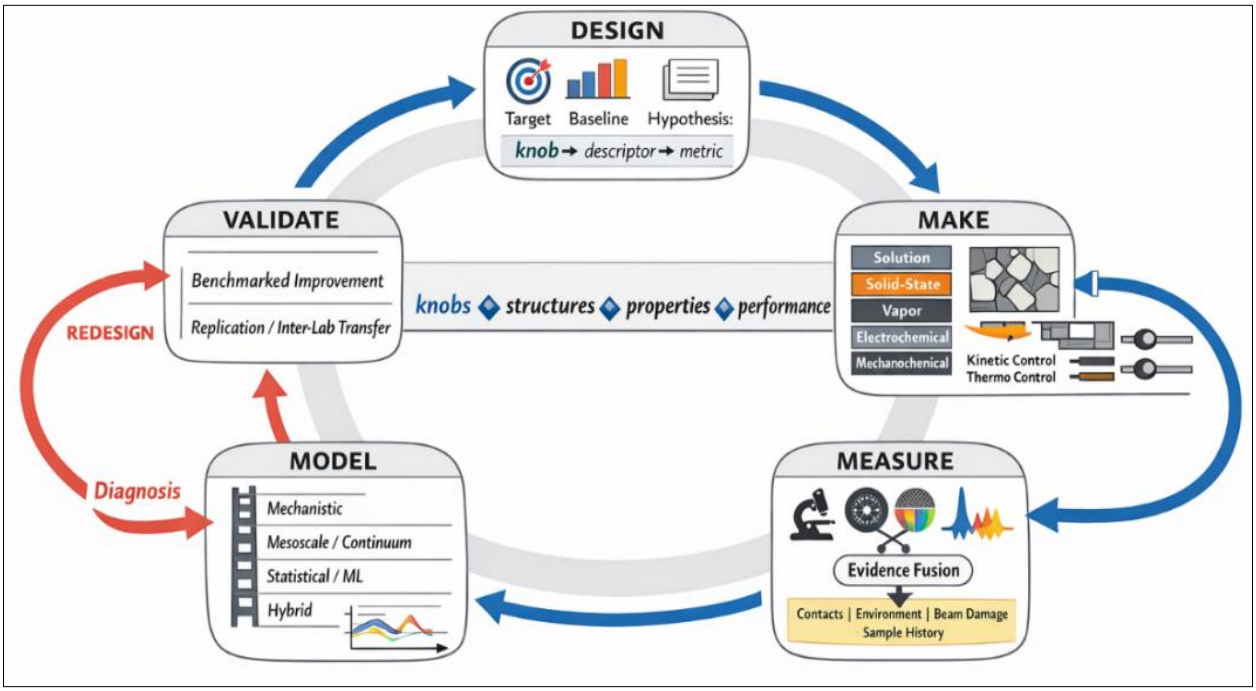

Figure 1: Cross-Scale Design Grammar Roadmap for Functional Matter: Design–Make–Measure–Model–Validate

Table 1: Scope map and key terms with quantitative anchors

Key term or scope anchor	Numeric anchor (typical)	Why it matters for this review	Included
Innovation to first use	10 to 20 years	Motivation for end-to-end workflows	Yes
XPS near-surface "information depth"	~10 nm for ~95% signal	Defines what surface chemistry means	Yes
ToF-SIMS sampling depth	1 to 2 nm	Contamination dominates if uncontrolled	Yes
AFM vertical resolution	<1 Å	Roughness claims need environment control	Yes

Key term or scope anchor	Numeric anchor (typical)	Why it matters for this review	Included
Extracted causal mechanisms at scale	207,200 mechanisms	Shows knowledge is scattered	Context
Supporting multimodal evidence at scale	1,113,940 evidences	Motivates evidence-fusion logic	Context
Materials knowledge graph scale	>70,000 entities; 5.4 million triples	Enables machine-actionable grammar	Context
Self-driving labs focus	closed-loop automation + AI	Forces formal definitions of knobs and metrics	Context
UQ emphasis in prediction	calibrated uncertainty methods	Prevents false "improvements" within noise	Yes
Causal inference in PSP links	intervention-focused causal effects	Makes results more transferable	Yes

2. The Cross-Scale Design Grammar Framework

A "design grammar" becomes useful only when it turns scattered facts into a repeatable causal workflow. In materials, the most widely used backbone is the process-structure-property-performance (PSPP) logic used in ICME-style thinking, where processing choices are expected to produce specific structures that then determine properties and ultimately performance (Goulding, 2018). This review extends that backbone in two ways: (i) it treats synthesis and processing as explicit operators that can be intervened upon (not only observed), and (ii) it treats every link as an inference statement with uncertainty and validation gates, so that "improvement" is defined as a causal and benchmarked effect, not a correlated change.

At the grammar level, each study can be decomposed into four unit types that are portable across domains.

- **Building Blocks (State Descriptors).** These are quantitative descriptors of what the material "is" at multiple scales: composition and stoichiometry; phase fractions; grain size and texture; pore size and connectivity; interphase thickness and chemistry; defect densities and distributions; surface roughness; junction geometry. A key rule is that a descriptor must be tied to an operational measurement domain. For example, "surface chemistry" in XPS is not an abstract concept but a near-surface signal typically discussed in terms of a characteristic information depth on the order of nanometers (Stevie, 2020).
- **Interactions (Mechanisms and Couplings).** These are the links that map descriptors to each other and to properties: nucleation and growth; diffusion and segregation; adsorption and charge transfer; percolation and tortuosity; stress and fracture; defect formation and migration; interface reactions and interphase evolution. The same descriptor can participate in multiple interactions, which is why "single variable" narratives often fail under transfer.
- **Constraints (Feasibility and Realism).** These include thermodynamic bounds (phase stability), kinetic ceilings (diffusion-limited formation), manufacturability (throughput and scale), safety and toxicity, and environment (humidity, oxygen, contaminants). Constraints decide which operators are even meaningful. For example, vapor-phase routes such as ALD are typically conducted at modest temperatures, commonly stated as below about 350 C, which constrains the accessible chemistries and defect equilibria (Johnson *et al*., 2014).
- **Metrics (What Counts as Function).** Metrics must be numerical and test-conditioned: conductivity at a stated temperature and stack pressure; catalytic turnover under stated potential, pH, and mass transport; mechanical toughness at a stated strain rate; stability as capacity retention over cycles with a specified protocol. The grammar treats metrics as a contract: no protocol, no transferable claim.

The second layer of the framework is causality. PSPP diagrams often imply causality, but the grammar makes it explicit by distinguishing **interventions** (changing a knob) from passive observation. Recent materials and reaction-engineering literature argues that causal inference can extract actionable cause-effect relationships among processing, structure, and property variables and make findings more actionable than correlation-only workflows (Ting *et al*., 2022). A complementary perspective emphasizes causal discovery plus causal inference as a way to identify plausible causal structures and then quantify intervention effects and reliability (Tian *et al*., 2025). In the grammar, the causal chain is written as:

Operators (Knobs) → State Descriptors (Structure, Interfaces, Defects) → Properties → Performance Metrics

And every arrow must be supported by evidence appropriate to that arrow. This is also where failure modes enter, because wrong arrows are usually created by confounding or artifacts.

Uncertainty is not an add-on in this framework. It is carried along the chain and separated into at least three practical sources: (i) measurement uncertainty and artifacts, (ii) process variability (batch-to-batch, microstructure stochasticity), and (iii) model-form

uncertainty (missing physics, poor generalization). In computational PSP workflows, uncertainty quantification is increasingly treated as integral because it determines whether predictions are actionable and whether calibration is honest (Pribe *et al*., 2023). In ML-based prediction, uncertainty quantification is similarly framed as critical for robust and generalizable property prediction rather than point accuracy alone (Varivoda *et al*., 2023).

A practical strength of defining the grammar units is that it makes "end-to-end" design possible, including inverse design. For example, generative modeling approaches have been proposed to represent the full PSP chain and support goal-oriented material design by linking processing parameters to latent microstructure representations and then to properties (Zang *et al*., 2025). The grammar does not require any single modeling method, but it requires that whatever model is used must connect to measurable descriptors and must pass validation gates.

Finally, the framework is designed to be machine-actionable without becoming a purely computational exercise. The FAIR Guiding Principles explicitly emphasize that data, tools, and workflows should be structured so machines can find and use them, not only humans (Wilkinson *et al*., 2016). This matters because the design grammar is meant to scale to modern high-throughput and closed-loop settings, where ambiguous variable definitions and missing metadata can overwhelm any optimization engine.

Table 2: Variable dictionary (controllable parameters vs measurable outputs) with numeric ranges

Variable class	Example variable (units)	Typical range (value)	Practical note for the grammar
Knob, solution route	Sol concentration (M)	0.05 to 2.0 M (Elferink *et al*., 1996).	Sets nucleation, gelation, pore evolution
Knob, vapor route	LPCVD pressure (Torr)	0.1 to 10 Torr (LPCVD overview, n.d.).	Controls gas-phase vs surface reactions
Knob, vapor route	LPCVD temperature (C)	200 to 800 C (LPCVD overview, n.d.).	Strong lever on kinetics and defects
Knob, ALD route	ALD temperature (C)	typically less than 350 C (Johnson *et al*., 2014).	Defines ALD window and impurity risk
Knob, ALD route	ALD growth per cycle (A/cycle)	typically less than 1 A per cycle (Johnson *et al.*, 2014).	Converts cycles to thickness, sets conformality control
Knob, PVD route	Sputtering working pressure (mTorr)	1 to 10 mTorr (Aalto University, n.d.).	Alters energy, scattering, film density
Knob, PVD route	Sputtering discharge voltage (V)	300 to 700 V (CAPST slides, n.d.).	Proxy for plasma energy regime
Knob, thermal history	Cooling rate (K/s)	10 to 250 K/s (Semiatin *et al*., 2018).	Controls precipitation and transformation pathways
Output, structure	Grain size classes	nanocrystalline up to ~100 nm; UFG ~0.1 to 0.3 um (Tjong, 2004).	Links processing to strength, transport, stability
Output, defects	Dislocation density (m^-2)	~10^9 to 10^10 m^-2 annealed; up to ~10^16 m^-2 heavily deformed (Dislocation density overview, n.d.).	Quantifies stored strain and failure risk
Output, interface	SEI thickness (nm)	typical ~20 nm (Cheng *et al*., 2016); reported 1.5 to 584 nm across studies (Andriunas *et al*., 2022).	Gates transport, impedance growth, degradation
Output, architecture	Metal foam porosity (percent)	75 to 95 percent void volume (Oshida, 2013).	Sets density, stiffness, permeability trade-offs
Output, surface	ALD film RMS roughness (nm)	~0.25 to 3.5 nm in reported cases (Schiliro *et al*., 2021; Rogozhin *et al*., 2021).	Flags morphology artifacts and contact effects
Property, transport	Sulfide SSE ionic conductivity (S/cm)	exceeds 1 mS/cm; examples 1.2e-2 to 2.5e-2 S/cm (Li *et al*., 2024; Man *et al*., 2025).	Sets rate capability, enables benchmarking
Property, electronic	Carrier concentration (cm^-3)	~1e16 to 1e18 lightly dopable (Stevanovic group, 2020); heavy doping effects near 1e19 to 1e20 (Doping density overview, n.d.).	Ties processing and defects to electronic function

3. Synthetic Pathways and Mechanistic Control

A cross-scale design grammar becomes actionable only when synthesis is treated as an explicit set of control operators that transform an intended chemical space into a realized microstructure state. In practice, the same target function (for example, ionic conductivity, catalytic activity, or device stability) can be reached by very different routes, but each route exposes a different subset of "knobs" (temperature-time histories, chemical potentials, transport fields, mechanical energy input) and therefore produces different families of microstructure distributions. The route family is therefore not just a processing choice; it defines the causal channel through which composition and energy are injected into matter and converted into phase fraction, grain size, defect populations, and interphase architectures. (Johnson *et al.,* 2014; LaMer & Dinegar, 1950; Whitehead *et al*., 2021).

Across most functional materials classes, it is useful to organize route families into five operator sets: solution, solid-state, vapor, electrochemical, and mechano-chemical. Each operator set has characteristic rate-limiting steps and therefore characteristic "dominant knobs". Solution routes typically couple supersaturation generation to nucleation and growth, so the principal control handles are concentration trajectories, injection or mixing rate, pH, ligands, and temperature history, all of which set nucleation burst timing and the subsequent growth regime (LaMer & Dinegar, 1950; Whitehead *et al*., 2021).

Solid-state routes are frequently constrained by diffusion across particle-particle contacts and by the progressive reduction of diffusion lengths through grinding, milling, and repeated calcination. As a result, the dominant knobs become particle size after mixing, degree of intimate contact, thermal ramp and dwell schedule, atmosphere, and precursor volatility. Even a seemingly simple decision such as whether powders are ground to around the 10 micrometer scale (or co-milled) can materially shift which phases appear first and which defects are frozen in during cooling. (West, 2014; Hamzaoui *et al*., 2020).

Vapor routes (CVD, PVD, ALD) are best interpreted as operators that control surface reaction vs gas-phase transport and thus can strongly shape conformality, thickness uniformity, and interface abruptness. For ALD specifically, sequential self-limiting surface chemistry gives sub-nanometer thickness control and high conformality, but the practical knob set becomes precursor chemistry, pulse and purge timing, substrate temperature window, and reactor hydrodynamics (Johnson *et al.,* 2014; Oviroh *et al*., 2019).

Electrochemical routes expose knobs that are difficult to access otherwise: electrochemical potential, current density, and mass transport fields control nucleation density, texture, morphology, and dendrite risk. In electrodeposition, microstructure can shift measurably within current density windows such as 10 to 100 mA/cm² in common nickel baths, while higher current densities can push toward rougher, nodular or cracked deposits depending on chemistry and agitation (Boukhoubiete *et al*., 2021; Arowolo *et al.,* 2020).

Mechano-chemical routes treat mechanical energy as a reagent. Ball milling and related mechanochemistry can accelerate reactions by creating fresh surfaces, defects, and local temperature spikes, but the route is notoriously sensitive to equipment-specific parameters. Critical knobs include ball-to-powder ratio (often in the 5:1 to 20:1 range), milling frequency (commonly tens of Hz in mixer mills), ball size and mass, jar material, and milling time, all of which co-determine reaction kinetics and contamination risk (Suryanarayana, 2001; Julien *et al*., 2017; Zakeri *et al*., 2012).

Within the design grammar, thermodynamic control and kinetic control are not abstract textbook labels. They function as a practical switch that determines whether your synthesis operator will preferentially realize the lowest-free-energy state accessible on experimental timescales or trap metastable structures that may be functionally beneficial. IUPAC defines thermodynamic control as conditions where product distributions reflect equilibrium constants, whereas kinetic control reflects relative formation rates under conditions where equilibration is limited (IUPAC, 2025a; IUPAC, 2025b). In materials synthesis, this distinction governs whether one expects equilibrium phase assemblages, larger grains and reduced defect densities (often favored by long anneals), or alternatively smaller grains, higher defect densities, and metastable polymorphs that can be performance-relevant. (IUPAC, 2025a; IUPAC, 2025b; Whitehead *et al*., 2021).

A useful operational interpretation is: thermodynamic control is often promoted by high temperature, long time, and sufficient mobility to equilibrate; kinetic control is promoted by short time, rapid quench, limited diffusion, or strong driving forces that outpace relaxation. The point for the review is not to privilege one regime, but to make the regime explicit in the causal chain. If a paper claims "defect-engineered performance" but uses processing schedules that likely anneal defects away, the claimed causal story is inconsistent unless the evidence shows defect persistence. Conversely, if a route claims equilibrium phase purity but uses short dwell times and poor mixing, the thermodynamic claim is weak without equilibrium checks (phase fraction vs time, or reversible transformations). (West, 2014; IUPAC, 2025a).

Scaling from benchtop to pilot to manufacturing is often treated as "keep the recipe, increase the batch size". That approach fails because most knobs do not scale linearly: mixing time, thermal gradients, mass

transfer coefficients, and residence time distributions change with geometry and throughput. In solution routes, scaling alters nucleation and growth because mixing time becomes comparable to or larger than nucleation burst times, changing dispersity and morphology. Real scale-up studies explicitly re-optimize temperatures, residence times, and workup steps and report yields and size distributions at the larger scale, rather than assuming invariance (Sukweenadhi *et al*., 2021).

In electrochemical systems, scale-up is often limited by achieving uniform current distribution and mass transport across larger electrodes. Flow cell design guidance commonly targets small interelectrode gaps such as 1 to 5 mm to reduce ohmic losses and improve transport, and scale-up analyses emphasize hydrodynamics, current distribution, and reactor geometry rather than only electrolyte composition (Pletcher *et al*., 2017; Pérez *et al*., 2020).

In mechanochemistry, scale-up has historically been constrained by batch ball milling, but continuous reactive extrusion (twin-screw extrusion) is increasingly used as a translation path from batch milling to flow processing, enabling controlled feed rates, temperature control, and steady-state operation (Bolt *et al*., 2022; Crawford *et al*., 2018). This matters for the grammar because it shows how an operator family can be "ported" across scales only when the operator is reparameterized in physically relevant terms (specific mechanical energy input, residence time, screw configuration), not by copying nominal rpm or time values across machines.

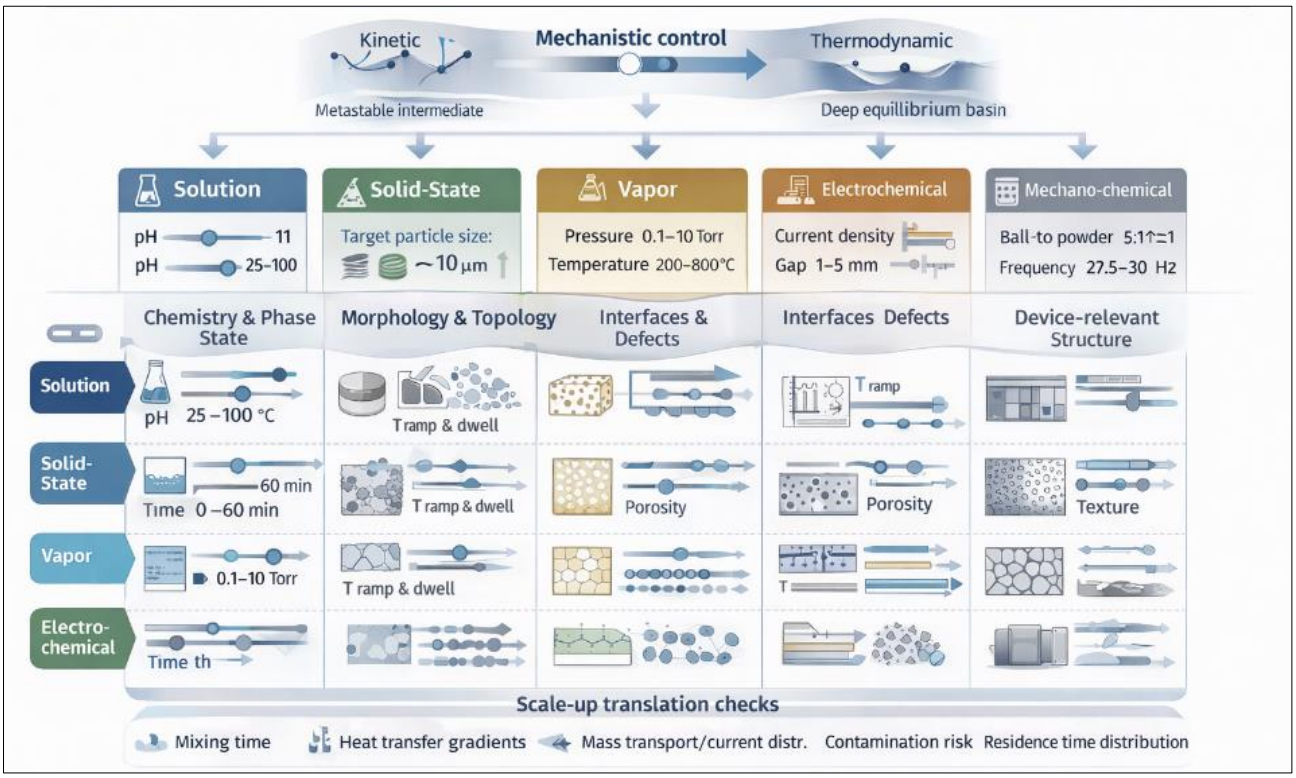

Figure 2: ***Synthesis Knobs to Microstructure Outcomes Map: Route Families as Control Operators***

Table 3: ***Minimum reporting checklist for synthesis and reproducibility metadata***

Route family	Minimum must-report metadata	Numeric fields that must be reported (units, example ranges)	Reproducibility metadata to include
Solution	Full recipe + order of addition; mixing protocol; atmosphere; workup (quench, wash, centrifuge)	pH 1–11; T 25–100 °C; time 0–60 min (representative parameter sweep ranges); concentrations (mM to M as used); centrifugation time (example 30 min)	Reagent supplier + purity; batch IDs; stirring rpm; vessel geometry; sampling timepoints; raw UV-Vis/XRD/TEM files if used for claims
Solid-state	Precursor forms; grinding/milling method; calcination schedule; atmosphere control	Particle size target after grinding (~10 µm); calcination threshold example where crystallization begins (~460 °C, material-dependent); ramp rate (°C/min) and dwell (h)	Crucible material; furnace model; gas composition and flow rate; cooling rate; number of regrinds; phase fraction vs dwell time if claiming equilibrium
Vapor (CVD)	Reactor type; precursor delivery; substrate prep;	LPCVD pressure 0.1–10 Torr; temperature 200–800 °C	Gas flow rates; substrate position; temperature

Route family	Minimum must-report metadata	Numeric fields that must be reported (units, example ranges)	Reproducibility metadata to include
	pressure control; exhaust handling		calibration method; thickness map across wafer; precursor purity and delivery temperature
Vapor (ALD)	Precursor and co-reactant; pulse/purge sequence; substrate temperature window	Film growth per cycle and total cycles (report nm or Å per cycle); temperature setpoint in ALD window	Pulse and purge times; carrier gas and flow; thickness uniformity and conformality metrics; reactor model
Electrochemical	Cell type; electrode materials; reference electrode; electrolyte composition; agitation/flow	Current density 10–100 mA/cm²; interelectrode gap 1–5 mm; potential vs reference (V)	Electrode area and geometry; separator pore size if used; iR compensation; temperature; flow rate; replicate runs
Mechano-chemical	Mill type; jar + ball material; sealing atmosphere; loading protocol	Ball-to-powder ratio 5:1–20:1; frequency 27.5–30 Hz; milling time (h); contamination example Fe 0.23–8 wt% reported across conditions	Jar temperature monitoring; cleaning protocol; media wear estimate; sample mass; pause schedule; post-milling sieving conditions

4. Assembly, Architecture, and Mesoscale Order

A cross-scale design grammar becomes practically useful when it tells you how to deliberately sculpt mesoscale order from nanoscale building blocks, then predict which functions that architecture will enable or suppress. Here, "architecture" includes pore hierarchy, connectivity, anisotropy, domain periodicity, grain or domain boundaries, and the spatial arrangement of phases across nano to macro length scales. In many functional systems, the dominant performance bottleneck is not the intrinsic material property, but how fast species, charges, photons, or stresses can move through the architecture and how robustly that architecture survives processing and operation. (Thommes *et al*., 2015).

A helpful starting point is to treat assembly as a set of operators that transform local interactions into global order. For self-assembly, the "operators" are typically encoded in chemistry and thermodynamics: amphiphile packing in solution, block incompatibility in block copolymers, entropic packing of colloids, and ligand mediated interactions. For directed assembly, operators include external fields, geometric confinement, patterned substrates, and imposed flow. Each operator changes which free-energy minima are accessible and how quickly the system can reach them, and each introduces characteristic defect families that must be anticipated and quantified. (Albert & Epps, 2010).

Porosity is the most universal architectural motif in functional matter, because it trades density for transport and interfacial area. To standardize the language, the IUPAC pore-size convention remains the most widely used: micropores are below 2 nm, mesopores are 2 to 50 nm, and macropores are above 50 nm, with "nanoporous" often referring broadly to pores below 100 nm. (Thommes *et al*., 2015). In practice, high-performance devices frequently require hierarchical pore systems that mix at least two regimes, for example mesopores for fast diffusion plus micropores for high surface area, or macropores as highways feeding nanostructured active regions. (Thommes *et al*., 2015).

The most instructive way to see architecture-function coupling is to contrast canonical architectures whose property ranges are well-established. Silica aerogels are an extreme case of nanoscale and mesoscale porosity: reported bulk densities span roughly 0.003 to 0.5 g/cm³, surface areas 500 to 1500 m²/g, porosity 80% to 98%, and mean pore diameters 2 to 50 nm. (Akhter *et al*., 2021). These values explain why aerogels excel at low thermal conductivity and large accessible surface, but also why they often suffer from fragility and processing sensitivity. (Akhter *et al.,* 2021).

Confinement and capillarity are the hidden couplers between assembly and defects, especially whenever a liquid is removed from a nanostructured network. In nanopores, the capillary pressure associated with a curved meniscus follows the Young–Laplace relationship, so the pressure scales inversely with pore radius. For water at room temperature, surface tension is about 72 mN/m, which implies that drying stresses can reach the MPa range for tens-of-nanometers pores and increase further as pores shrink. (Liu & Cao, 2016). This is the physical reason why "perfect" nanoscale architectures often crack, shrink, or collapse unless drying is engineered (for example, supercritical drying or surface modification) or the network is reinforced. (Akhter *et al*., 2021; Liu & Cao, 2016).

At the other end, macroporosity and directional mesoscale order can be intentionally imposed to create transport anisotropy. Freeze casting (ice templating) is a clear example where processing generates oriented pore channels. In a large review and associated database analysis, reported pore widths span from below 1 μm up to about 400 μm for roughly 60% porosity materials, and strong gradients can occur along the freezing direction if

conditions are not uniform. (Scotti & Dunand, 2018). These numeric ranges matter because they set diffusion lengths, permeability, and mechanical anisotropy, which in turn decide whether an architecture is suitable for electrodes, filtration, or tissue scaffolds. (Scotti & Dunand, 2018).

Directed assembly is the most direct way to convert the design grammar into reproducible mesoscale order. Block copolymer self-assembly is a cornerstone because it naturally produces periodic domains with characteristic sizes on the order of 10 to 100 nm, and thin-film geometries around 100 nm thickness are common in device-relevant contexts. (Albert & Epps, 2010). Directed self-assembly (DSA) then uses top-down guides to reduce defects and lock in desired symmetry. Literature examples explicitly demonstrate an 11.7 nm half-pitch block copolymer assembled in sub-10 nm resolution guiding patterns, and other demonstrations report well-resolved 5 nm half-pitch features in thin films for pattern transfer, illustrating how "architecture operators" can push into regimes where transport, optics, and electronic length scales are directly engineered. (Gottlieb *et al*., 2019; Lane *et al*., 2017; Jeong *et al*., 2013).

Field-directed assembly provides a complementary operator that is especially powerful for anisotropic fillers and percolating networks. Magnetic alignment can work even at surprisingly low fields when fillers are made responsive. A reported example aligns graphene nanoplatelet hybrids in epoxy using a magnetic field as low as 0.009 T before gelation, and related studies operate in the 0.5 T regime to modify composite properties during formation. (Wu *et al*., 2016). Architectural alignment is not only about orientation, it changes network connectivity and thus the percolation landscape. For carbon-nanotube polymer composites, literature surveys report electrical percolation thresholds as low as 0.04 wt% in some systems, with rheological thresholds around 0.1 wt%, and maximum conductivities reported up to 10,000 S/m at high filler loadings in selected matrices. (Bauhofer & Kovacs, 2008). These quantitative ranges help you decide whether "alignment" should be pursued for conductivity, toughness, or both. (Bauhofer & Kovacs, 2008; Wu *et al*., 2016).

Finally, colloidal and templated assembly bridges meso to macro through packing and replication. Inverse opal architectures, created by templating ordered colloidal spheres, explicitly span template sphere diameters from about 200 nm up to 10 µm in reported photonic crystal contexts, giving a direct geometric dial for photonic and transport length scales. (Ahmad *et al*., 2018). However, defect sensitivity can be extreme: work on convective colloidal assembly reports that achieving high ordering can require substrate roughness below about 30% of the bead diameter, and low concentration conditions can produce stripe patterns rather than uniform crystals. (Lebrun *et al*., 2014). In the grammar view, these are constraints that must be designed around, not surprises discovered after fabrication.

Table 4: Assembly tools, typical numeric operating windows, and common artifacts

Assembly / architecture tool	**Typical achieved length scale (examples)**	**Practical control "knobs" with numeric ranges**	**Typical artifacts and a quantitative diagnostic**
Block copolymer self-assembly (thin films)	Domain periodicity ~10 to 100 nm; film thickness ~100 nm	Polymer selection sets intrinsic pitch; annealing and surface energetics tune orientation (Albert & Epps, 2010; EMRS, 2018)	Dislocations, mixed orientation; quantify with GISAXS or SEM defect density over area (Albert & Epps, 2010)
Directed self-assembly (DSA) of block copolymers	Demonstrated 11.7 nm half-pitch in sub-10 nm guiding patterns; also 5 nm half-pitch reported	Guide pattern CD and pitch near polymer half-pitch; top-down registration quality (Gottlieb *et al*., 2019; Lane *et al*., 2017)	Line-edge roughness, missing or merged domains; quantify half-pitch distribution and placement error (Gottlieb *et al*., 2019)
Silica aerogel networks (sol-gel + drying)	Mean pore diameter 2 to 50 nm; surface area 500 to 1500 m^2/g	Density 0.003 to 0.5 g/cm^3; porosity 80% to 98% depends on precursor ratio and drying route (Akhter *et al*., 2021)	Shrinkage and cracking; track bulk density change and linear shrinkage; link to capillary-stress risk (Akhter *et al*., 2021; Liu & Cao, 2016)
Freeze casting (ice templating)	Pore width <1 to ~400 µm at ~60% porosity	Freezing rate and thermal gradient set lamella spacing and gradients (Scotti & Dunand, 2018)	Pore gradient and anisotropy; quantify pore-width histogram vs position using micro-CT (Scotti & Dunand, 2018)
Colloidal crystal / inverse opal templating	Sphere diameter range ~200 nm to 10 µm	Evaporation rate, concentration, substrate quality; roughness target <0.3× bead diameter for good ordering (Lebrun *et al*., 2014; Ahmad *et al*., 2018)	Cracks, domain boundaries, stripes; quantify domain size and crack spacing; report ordering metric from FFT of SEM (Lebrun *et al*., 2014)

Assembly / architecture tool	Typical achieved length scale (examples)	Practical control "knobs" with numeric ranges	Typical artifacts and a quantitative diagnostic
Field-assisted alignment (magnetic) for conductive or tough networks	Network-scale alignment over mm–cm parts	Magnetic field as low as 0.009 T can align responsive fillers before gelation; higher fields (0.5 T) used in other composite processing (Wu *et al.,* 2016)	Aggregation or incomplete alignment; quantify anisotropy factor from SAXS or conductivity ratio parallel vs perpendicular (Wu *et al*., 2016; Bauhofer & Kovacs, 2008)

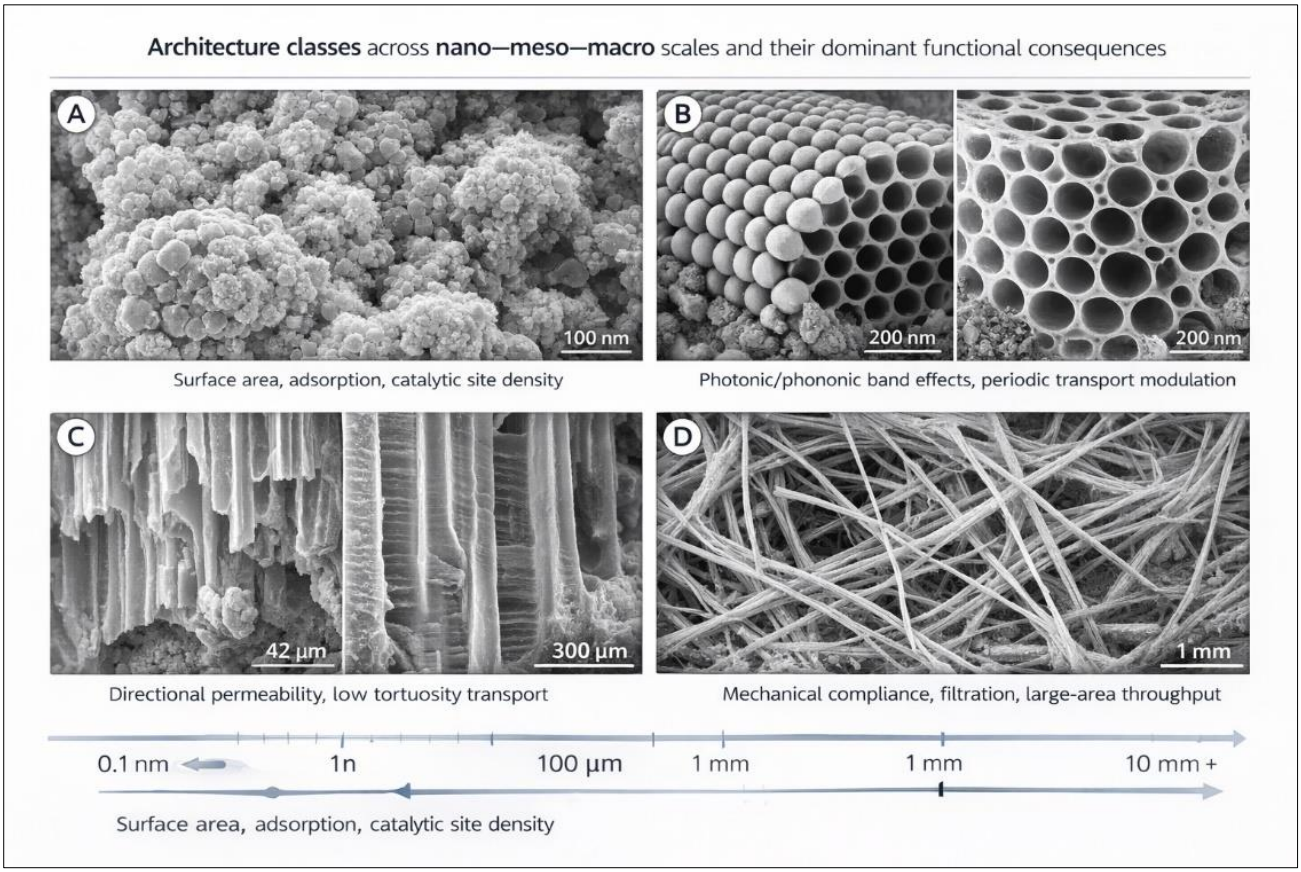

Figure 3: Architecture classes across nano–meso–macro scales and their dominant functional consequences

Representative micrographs illustrate how mesoscale order converts local interactions into system-level function. (A) Nanoscale porous aggregates and high-curvature networks highlighting surface-area dominated behavior relevant to adsorption and catalytic site density. (B) Periodic templated architectures (inverse-opal type ordering) showing long-range periodicity that can couple to photonic and transport modulation through controlled void geometry. (C) Directionally aligned channel or lamellar architectures representative of freeze-cast or templated scaffolds that reduce tortuosity and enable anisotropic permeability and directional transport. (D) Macroscale fibrous networks representative of nonwoven mats or electrospun architectures supporting mechanical compliance and high-throughput filtration, with performance governed by network connectivity and pore size distribution. The bottom scale axis emphasizes that architecture-design operators act across orders of magnitude, and that functional metrics often shift from surface-area control at the nanoscale to transport and mechanics control at meso to macro length scales.

5. Interfaces and Interphases as Function Gatekeepers

In functional matter, the interface is the boundary condition that the bulk is forced to obey. A catalyst can have a perfect bulk crystal but fail if adsorbates poison active sites. A semiconductor can have high mobility but deliver low current if the metal contact injects poorly. A solid electrolyte can have high ionic conductivity yet short-circuit if mechanical contact and interphase chemistry at Li|SE are unstable. In practice, performance bottlenecks often collapse onto a few nanometers at the surface, because that region simultaneously sets (i) thermodynamic driving forces (wetting, adsorption, segregation), (ii) kinetic barriers (charge transfer, desolvation, nucleation), and (iii) transport through any reaction product layer (SEI/CEI,

passivation oxide, space-charge region). (Bormashenko, 2016; Jagger & Pasta, 2023).

A useful "design grammar" view is to treat interface engineering as selecting a small set of operators that rewrite boundary conditions: surface termination and functional groups, roughness and porosity, interlayer or coating chemistry, dopant segregation, junction band alignment, and mechanical preload. Each operator changes a measurable interface state variable: surface energy and contact angle (wetting and infiltration), interfacial reaction rate constants (often summarized through exchange current density or charge-transfer resistance in electrochemical systems), and the effective resistance of interphases that act like series elements. This framing is not cosmetic. It converts fuzzy statements like "interface matters" into testable claims: if we changed termination X to Y, the contact angle changed, the real contact area changed, then interfacial impedance and stability changed in a predictable direction. (Bormashenko, 2016; Bard & Faulkner, 2001).

Interphases deserve special emphasis because they are not simply "thin coatings". Many form spontaneously and evolve during operation. In batteries, the SEI and CEI are reaction products that must be electronically insulating but ionically permissive, mechanically tolerant, and chemically stable. A key trap is that the interphase you measure can depend on the state you preserved. Cryogenic methods show that SEI thickness can differ between "dry" and electrolyte-present states. One widely cited cryo-EM study reported a roughly ~20 nm SEI when preserved in vitrified electrolyte but about ~10 nm when characterized in the absence of liquid electrolyte, indicating swelling and state dependence rather than a single fixed thickness. (Zhang *et al*., 2022). On the cathode side, desired CEI thickness is often discussed in the 5–50 nm range in the context of stabilizing aggressive high-energy cathodes while maintaining Li+ transport. (Wu *et al*., 2021). These numbers are not "targets" by themselves, but they anchor what is physically plausible for transport and mechanical compliance.

Interfaces also gate function through junction physics. In electronic materials, the figure of merit is frequently specific contact resistivity (ρc) rather than bulk conductivity. Even in wide-bandgap and high-power materials, literature shows that low-resistance ohmic contacts are commonly discussed in the 10^-6 to 10^-5 Ω·cm^2 range for practical device relevance. (Roccaforte *et al*., 2016). In electrochemical and mixed-conducting systems, analogous "contact penalties" appear as constriction resistance, interfacial charge transfer resistance, and interphase resistances. Mechanically, solid-state stacks introduce another coupling: preload changes real contact area, void evolution, and therefore interface resistance and stability. Modeling and review work on Li|solid-electrolyte contacts suggests that stack pressure can be a stabilizing control knob, with recommendations on the order of tens of MPa in some contexts, while other datasets show that comparatively low pressures can be sufficient depending on materials and geometry. (Zhang *et al*., 2020; Chen *et al*., 2021).

Many reported "interface gains" are measurement artifacts. Three failure modes recur across subfields:

- **Contact Artifacts (Electrical and Thermal):** Two-probe resistance folds together sample resistance and contact resistance, so an apparent improvement can be only better probing or clamping. Four-point methods suppress contact resistance contributions and are usually the correct baseline when feasible. (Suragus, 2025).
- **Nonlinear or Invalid Impedance Spectra:** Electrochemical impedance spectroscopy assumes a pseudo-linear response. Standard practice is to use small perturbations, commonly 5–10 mV, and then validate linearity and causality using tools such as Kramers–Kronig checks. (Brett *et al*., 2022; Metrohm, 2019).
- **Environment and Handling:** Air and trace moisture can rewrite the surface faster than your measurement. For Li-metal and sensitive interphases, many studies assemble and store materials under very dry inert conditions, for example gloveboxes reported at H2O and O2 < 0.1 ppm, and they use sealed transfer holders for post-mortem tools to avoid "measurement-created interphases". (Kühn *et al*., 2023).

Table 5: Interface metrics and best-practice test conditions

Interface metric (what it diagnoses)	Typical value or range (reported)	Best-practice test condition to report	Common pitfall that fakes improvement
EIS perturbation amplitude (linearity)	5–10 mV	Confirm linear region, report amplitude and check with Kramers–Kronig	Using too large amplitude causes harmonics and nonphysical fits
EIS frequency window (process separation)	~100 kHz to ~10 mHz	Report full range and points-per-decade	Truncating low-f limits hides diffusion or interphase growth
Double-layer capacitance (electroactive area proxy)	~50–100 µF·cm^-2	Normalize to geometric area and report roughness factor if known	Comparing unnormalized Cdl across different areas

Interface metric (what it diagnoses)	Typical value or range (reported)	Best-practice test condition to report	Common pitfall that fakes improvement
"Dry-state" SEI thickness on Li (state dependence)	~10 nm	Specify preservation state (dry vs vitrified), cryo handling	Air exposure thickens/changes SEI before measurement
"Wet/vitrified" SEI thickness on Li	~20 nm	Specify electrolyte present and vitrification protocol	Mixing dry and wet measurements as if equivalent
Desired CEI thickness in some high-energy contexts	~5–50 nm	Report how thickness was inferred (TEM, XPS depth, ToF-SIMS)	Claiming "stable CEI" without thickness or composition evidence
ALD coating thickness often cited as optimal on cathodes	~1–2 nm (Al2O3); ~1 nm (ZrO2); <1 nm (TiO2)	Report thickness, chemistry, and post-cycling retention	Coating reduces performance due to blocking if too thick, but not reported
Li	solid-electrolyte stack pressure used to manage contact	Example outcomes at 5–25 MPa reported	Report pressure, fixture compliance, and pressure history
Specific contact resistivity for practical low-R ohmic contacts (example: SiC)	~10^-6 to 10^-5 Ω·cm^2	Report extraction method (TLM/CTLM), anneal, doping	Reporting only total resistance hides contact domination
Glovebox environment for reactive interfaces	H2O, O2 < 0.1 ppm (reported)	Report O2/H2O levels, exposure time, transfer protocol	"Dry room" vs glovebox differences alter interphase chemistry

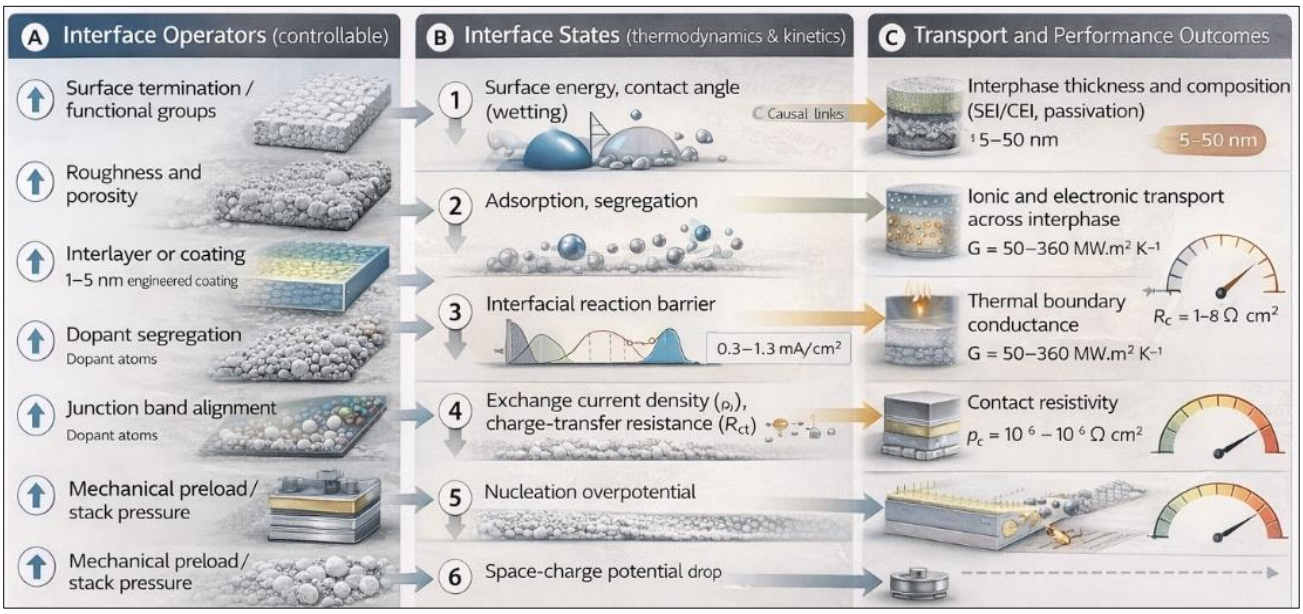

Figure 4: Interface and interphase map linking chemistry and structure to transport and performance

The schematic organizes interface control into three coupled layers. (A) Interface operators (controllable) such as surface termination or functional groups, roughness and porosity, engineered interlayers or coatings (typically 1–5 nm), dopant segregation, junction band alignment, and mechanical preload or stack pressure. (B) Interface states (thermodynamics and kinetics) including wetting behavior (surface energy and contact angle), adsorption and segregation, interfacial reaction barriers, and kinetic descriptors such as exchange current density and charge-transfer resistance, together with nucleation overpotential and space-charge potential drop. (C) Transport and performance outcomes governed by interphase thickness and composition (SEI/CEI or passivation, commonly 5–50 nm), ionic and electronic transport across the interphase, thermal boundary conductance, and specific contact resistivity, which ultimately determine power capability, efficiency, lifetime, and stability. The bottom band highlights frequent measurement confounders (two-probe vs Kelvin four-probe contacts, EIS excitation amplitude and validity checks, atmosphere control such as O2/H2O at low ppm levels, and pressure/temperature control) that can mimic interface "improvements" if not explicitly controlled and reported.

6. Defects, Disorder, and Degradation Pathways

Defects are not a special case in functional matter. They are the default state once you process, cycle, illuminate, bias, stress, or expose a material to reactive

environments. A cross-scale grammar treats defects as structured variables that connect nanoscale chemistry to macroscale reliability: point defects (vacancies, interstitials, antisites), line defects (dislocations), planar defects (grain boundaries, stacking faults), and volumetric defects (voids, pores, second phases, cracks). What makes defects powerful is that they couple fields that are otherwise treated separately. A vacancy can change local charge state, lattice strain, and diffusion. A dislocation can channel fast diffusion and act as a chemical sink. A grain boundary can be both a short-circuit path and a barrier depending on segregation and space-charge effects.

Formation is the first branch in the defect landscape. At equilibrium, formation is governed by formation free energies and chemical potentials, but most functional materials are kinetically trapped. That is why synthesis conditions can lock in "non-equilibrium defect chemistries" that later relax during operation. In oxide perovskites, oxygen vacancy formation energies are a central microscopic descriptor because they set the accessible vacancy concentration and therefore transport and redox behavior (Wexler *et al*., 2021). In metals and alloys, processing routes such as cold work and additive manufacturing can generate dislocation networks many orders of magnitude higher than well-annealed crystals, and that defect inventory changes mechanical response and diffusion-controlled aging.

Migration and interaction define the second branch. Defects rarely stay where they form. Vacancy-mediated diffusion and defect drift under electric fields or stress gradients are often rate-limiting steps for degradation. Atomistic studies in oxides frequently report oxygen-vacancy migration barriers on the order of ~0.5 to 0.6 eV in representative layered oxides, which is enough to make transport extremely temperature sensitive through Arrhenius factors (Mastrikov *et al*., 2025). In parallel, extended defects can provide fast pathways. Dislocations can enhance vacancy motion relative to bulk, so a microstructure that is "mechanically acceptable" may still be "chemically leaky" if it creates fast highways for diffusion (Defects and dislocations in MgO, n.d.).

Defects as levers versus liabilities is where design grammar becomes practical. Defects are levers when they are measurable, controllable, and coupled to the desired function with a stable operating window. A classic lever is deliberately tuning vacancy populations to enable ionic transport or catalytic activity, provided the defect population does not trigger phase changes or runaway chemical expansion. Defects become liabilities when they couple into positive feedback loops: vacancy creation increases electronic leakage, leakage increases local heating or side reactions, side reactions create more defects. The numbers matter. Well-annealed crystals can have dislocation densities around 10^10 m^-2, while heavily deformed or cold-rolled states can reach ~10^14 to 10^15 m^-2, changing both mechanical strength and diffusion behavior (Dohmen, 2010; Prochaska *et al*., 2023).

Degradation pathways are the "defect dynamics under operating constraints." Many systems show interphase growth, voiding, cracking, or chemical segregation that is invisible if you only inspect pristine samples. In batteries, even the apparent thickness of the solid electrolyte interphase depends on state and preservation: cryogenic studies report about 10 nm in a dry-state condition and about 20 nm when vitrified electrolyte is preserved, indicating swelling and state dependence that directly affects impedance and failure interpretation (Zhang *et al*., 2022; Zhang *et al*., 2022). Environmental handling is another common trap. Short air exposure measurably shifts interphase composition in lithiated battery components, so "post-mortem" data can inadvertently describe air reactions rather than operational degradation (Malmgren *et al.,* 2013).

Failure analysis and stability design complete the loop by converting defect stories into evidence that survives peer review. Practically, this means reporting defect claims with quantification, uncertainty, and at least one independent cross-check. It also means being honest about boundary definitions. For example, EBSD grain-boundary maps depend on a user-defined misorientation threshold, commonly 10° to 15° for defining grain boundaries and separating low-angle from high-angle boundaries (Mingard *et al*., 2006; Oxford Instruments, n.d.). For aging, accelerated degradation is powerful but dangerous if extrapolated blindly. Arrhenius-based lifetime prediction is widely used, yet guidance documents emphasize that activation energies and acceleration factors must be justified and documented, and that multi-temperature datasets are needed for credible fits (Maxwell *et al*., 2005; U.S. Nuclear Regulatory Commission, 2018; Le Saux *et al*., 2014).

Table 6: Minimum evidence checklist for defect claims with quantification

Defect claim (example wording)	Minimum evidence you must show	Quantification values you should report (with typical anchors)	Confounder to control
"Vacancy-type point defects increased"	At least 2 independent modalities (for example PAS + spectroscopy or transport)	PAS is sensitive to vacancy-type defect concentrations down to ~10^-7 (fractional concentration scale reported in PAS literature); report concentration and anneal history	Surface contamination or air exposure changes apparent defect chemistry

Defect claim (example wording)	Minimum evidence you must show	Quantification values you should report (with typical anchors)	Confounder to control
"Vacancy mobility is enhanced"	Arrhenius analysis across multiple temperatures plus a structural or chemical cross-check	Report activation energy; example oxygen-vacancy migration barriers ~0.5–0.6 eV have been reported in representative oxides	Limited temperature range gives non-unique activation energy
"Dislocation density explains performance change"	Direct dislocation metric (XRD line-profile, TEM, or validated EBSD method) plus processing history	Report dislocation density; annealed crystals can be ~10^10 m^-2, heavily deformed states can reach ~10^14–10^15 m^-2	Grain size and texture can mimic dislocation broadening
"Grain boundary engineering reduced fast paths"	EBSD boundary map with stated threshold plus chemistry at boundaries if segregation is claimed	Report misorientation threshold used (commonly 10°–15°) and grains counted (example guidance suggests hundreds of grains)	Changing threshold changes boundary fraction and conclusions
"Interphase growth is the dominant degradation mode"	Thickness plus composition evidence, ideally with state-preserving methods if sensitive	Report thickness and state: example SEI thickness about 10 nm (dry cryo) vs about 20 nm (vitrified electrolyte)	Drying, washing, or air exposure rewrites the interphase
"Lifetime prediction is Arrhenius-governed"	Multi-temperature accelerated aging with documented activation energy basis	Report temperatures used, activation energy, fit uncertainty; accelerated aging guides recommend using multiple temperatures and documenting the basis	Extrapolation beyond mechanism validity breaks predictions

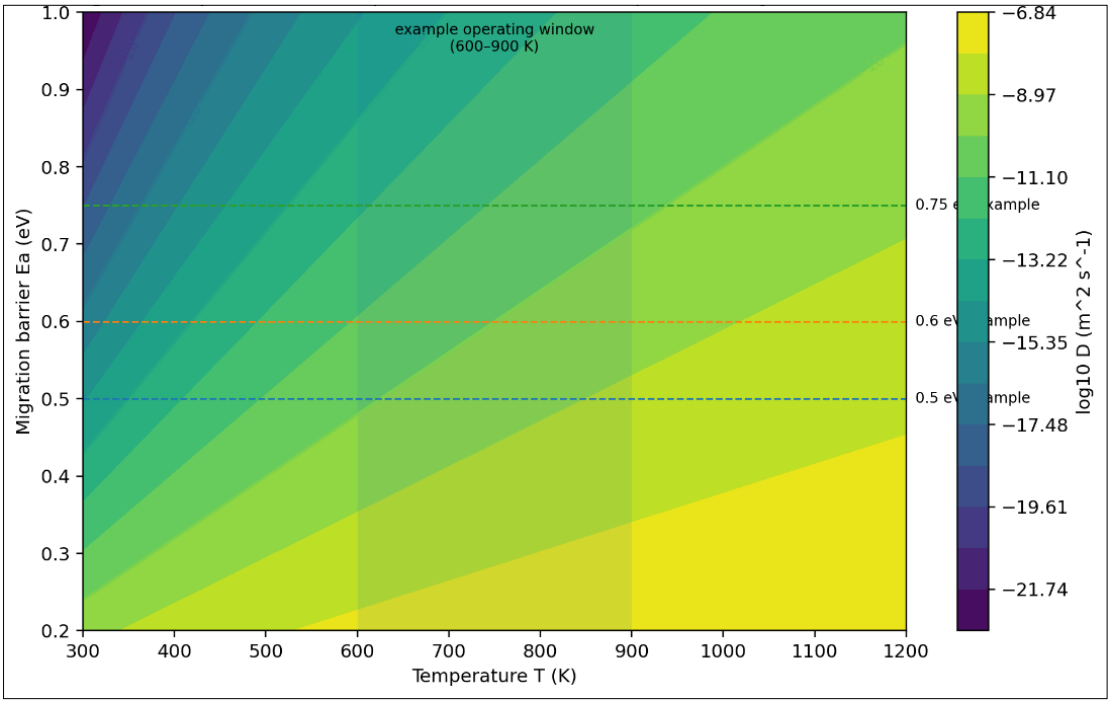

Figure 5: Defect kinetics map: diffusivity sensitivity to temperature and migration barrier

2D kinetics map showing log10 diffusivity D as a function of temperature (T) and migration barrier (Ea) using Arrhenius scaling. Horizontal dashed lines mark representative oxygen-vacancy migration barriers reported around 0.5 eV, 0.6 eV, and 0.75 eV across oxide/perovskite systems and conditions, illustrating how small barrier shifts cause orders-of-magnitude mobility changes (Mayeshiba *et al*., 2016; Mastrikov *et al*., 2025; Akkopru-Akgun *et al*., 2025).

7. Multimodal Characterization and Predictive Modeling

A cross-scale design grammar only becomes operational when characterization is treated as an inference problem rather than a collection of separate instruments. Each technique produces a signal that is filtered by physics, geometry, and sampling bias. The scientific claim is an inferred latent state, for example interphase composition, local coordination, defect population, percolation connectivity, or evolving phase fraction. If we do not explicitly map signal to claim, we

risk "instrument-specific truth" where different tools appear to contradict each other simply because they sample different depths, timescales, or environments (Baer *et al*., 2019; Racz *et al*., 2025).

Multimodal characterization solves this by constraining the same latent state with complementary projections. A practical rule is to pair at least one tool that is chemically specific (what is present), one that is structurally specific (how atoms or domains are arranged), and one that is morphologically or topologically specific (how the network is connected across length scales). This is increasingly implemented as "fusion measurement campaigns" at large-scale facilities where synchrotron datasets such as XANES, EXAFS, XRD, SAXS, PDF, and photoelectron spectroscopies are acquired as a coordinated bundle and then interpreted jointly with machine learning or physics-guided inversion, rather than as isolated snapshots (Baliyan *et al*., 2025; Barah *et al*., 2025).

Operando logic is the missing piece that prevents misleading structure-property narratives. In situ means the material is probed under a relevant condition. Operando adds simultaneous performance readout, such as product analysis for catalysis or electrochemical metrics for batteries, so that structural states are directly linked to function rather than assumed to be relevant (Portela, 2018; Prajapati *et al*., 2025). This distinction matters because many functional interfaces are transient. A catalyst surface can restructure within seconds under bias, and battery interphases can swell, dissolve, or densify depending on electrolyte and operating point. If the "characterized interface" is not the "working interface," the inferred mechanism becomes non-transferable (Alsaç *et al.,* 2025; Prajapati *et al*., 2025).

Modern operando tools now resolve timescales that overlap with real dynamic events. Synchrotron XAS can reach time resolutions from seconds down to milliseconds depending on configuration, which enables tracking oxidation state and coordination changes during operation rather than averaging them away (Genz *et al*., 2024; Lin *et al*., 2020). For mesoscale assembly and thin-film ordering, grazing-incidence scattering can be time-resolved as well. Reports demonstrate in situ GISAXS with temporal resolution around 200 ms for self-assembly processes, allowing kinetics and defect emergence to be quantified rather than guessed (Saxena *et al*., 2020; Posselt, 2017).

Because sampling depth differs drastically across techniques, fusion must explicitly encode "where" each instrument looks. Laboratory XPS is typically sensitive to roughly the outer 1 to 10 nm depending on conditions and material, which is ideal for surface termination and near-surface oxidation state, but insufficient for buried interphases without depth profiling or hard X-rays (Baer *et al*., 2019; Racz *et al*., 2025). ToF-SIMS is even more surface sensitive, often sampling roughly the top 1 to 2 nm, which makes it excellent for fragile adsorbate or interphase fragments but extremely vulnerable to contamination and handling artifacts (Graham *et al*., 2023). For buried interfaces, HAXPES can extend information depth beyond about 30 nm relative to classical XPS, enabling non-destructive access to deeper regions when geometry and signal permit (Seah *et al*., 2014). At the atomic scale, STEM-EELS can map chemical and electronic structure with sub-nanometer spatial resolution, with reviews reporting unit-cell scale mapping near ~0.4 nm and energy resolution around 0.1 to 0.3 eV in modern implementations, but it requires careful control of beam damage and representativeness (Gloter *et al*., 2017).

The core deliverable of a multimodal pipeline is not "more plots." It is a traceable chain: signals → features → physical inversion or learned mapping → claim with uncertainty. That uncertainty must include both measurement noise and model-form uncertainty, because even a perfect instrument cannot compensate for an incorrect forward model. This is why best-practice operando papers emphasize not just instrumentation, but also controls, validation of assumptions, and transparent reporting of what is and is not uniquely identifiable from the data (Prajapati *et al*., 2025; Petersen *et al*., 2022).

Predictive modeling in this design grammar should be framed as a ladder, where each rung trades fidelity for scale and speed. Mechanistic models (DFT, kinetic Monte Carlo, microkinetics) are interpretable and can reveal causal bottlenecks, but they require careful parameterization and often need calibration to connect to experiment. Continuum models (phase-field, transport PDEs, electro-chemo-mechanics) can connect microstructure to device behavior but are sensitive to boundary conditions that are often interface-controlled. Statistical and machine learning models can accelerate mapping from structure descriptors to properties, but they need explicit uncertainty quantification to be decision-ready and transferable across labs and domains (Tiep *et al*., 2023; Genz *et al*., 2024).

Two families of tools make this ladder credible: calibration and VVUQ (verification, validation, and uncertainty quantification). Bayesian calibration formalizes how uncertain model parameters and model discrepancy should be updated using experimental data, rather than hand-tuning until a curve looks right (Kennedy & O'Hagan, 2001). VVUQ frameworks then separate numerical correctness (verification) from agreement with reality (validation), and require that predictive uncertainty include contributions from numerical error, parameter uncertainty, and model-form uncertainty (Roy & Oberkampf, 2011). In ML, calibration has an analogous meaning: predicted uncertainties must be statistically reliable, because high accuracy does not guarantee trustworthy confidence estimates. Reliability diagrams and newer criteria for

conditional calibration highlight why uncertainty must be validated, not assumed (Bénard *et al*., 2023).

A practical way to embed this into your review is to require that every "prediction" shown in a case study includes: (i) the training domain and the application domain, (ii) an uncertainty estimate, (iii) at least one out-of-domain stress test, and (iv) a validation comparison against an experimental quantity that was not used for fitting. This aligns the modeling ladder with the design grammar goal: making decisions, not just fitting curves (Roy & Oberkampf, 2011; Kennedy & O'Hagan, 2001).

Table 7: Modality-to-claim mapping with quantitative ranges and recommended pairings

Target claim	Primary modality and typical window	Complementary modality to close identifiability gaps	Best-practice condition to report	Common artifact that breaks the claim
Surface termination, oxidation state, passivation chemistry	XPS sampling depth typically ~1 to 10 nm (Baer *et al*., 2019; Racz *et al*., 2025)	ToF-SIMS top ~1 to 2 nm for fragments and adsorbates (Graham *et al*., 2023)	Charge compensation, take-off angle, transfer protocol, sputter conditions if depth profiling	Preferential sputtering and ion damage in depth profiling, plus adventitious contamination
Buried interphase composition and gradients	HAXPES can extend information depth beyond ~30 nm vs classical XPS (Seah *et al.*, 2014)	Cross-section STEM-EELS mapping near unit-cell scale (~0.4 nm) with energy resolution ~0.1 to 0.3 eV (Gloter *et al*., 2017)	Geometry, photon energy, fitting model for peak deconvolution	Over-interpreting deconvolution without standards, plus beam damage in TEM
Operando oxidation state and coordination evolution	Synchrotron XAS time resolution can reach milliseconds to seconds depending on setup (Genz *et al.,* 2024); seconds-resolved operando demonstrated (Lin *et al.*, 2020)	Operando product or performance measurement, plus diffraction for phase fraction	Simultaneous activity readout and control experiments for mass transport limits	Mis-assigning active phase due to averaging, or measuring under non-representative transport regime
Mesoscale assembly kinetics, domain growth, ordering	In situ GISAXS temporal resolution reported ~200 ms in self-assembly studies (Saxena *et al*., 2020)	GIWAXS for crystallinity and orientation, plus microscopy for defect mapping	Beam footprint, incidence angle, solvent or vapor environment	Misinterpreting scattering without a validated structural model
3D connectivity, tortuosity, crack or pore network evolution	Micro-CT: industrial 50 to 100 µm; synchrotron CT 1 to 50 µm, with lab submicron systems reported (micro-CT overview)	FIB-SEM tomography for higher resolution sub-volumes	Voxel size, segmentation method, representative volume justification	Segmentation bias and insufficient representative volume
Local disorder and short-range structure in nanomaterials	Atomic PDF methods capture local structure and disorder (Billinge, 2019; Terban *et al*., 2021)	Pair with XAS for coordination chemistry or TEM for real-space validation	Q-range and data reduction protocol	Non-unique fits if constraints are weak, overfitting multiple phases

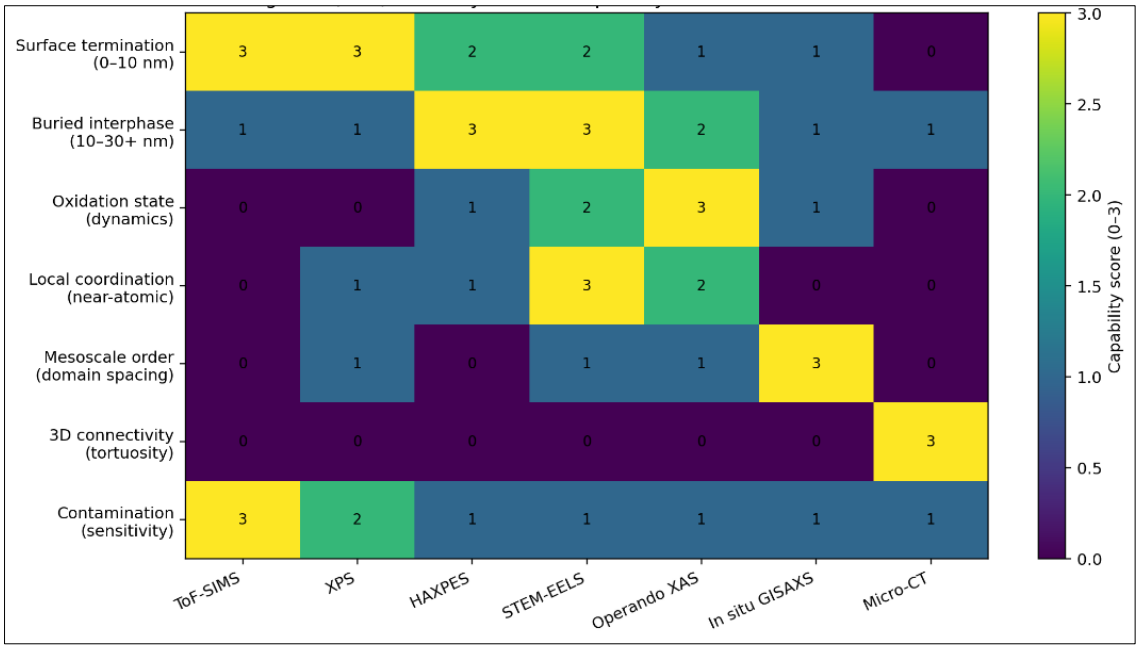

Figure 6: Modality to claim capability matrix for evidence fusion

Figure 7. A decision-ready heatmap that converts "multimodal characterization" into an explicit claim coverage plan. Rows represent common latent claims (surface termination, buried interphase chemistry, oxidation-state dynamics, local coordination, mesoscale order, 3D connectivity, and contamination sensitivity). Columns represent common modalities. Cell values are capability scores (0 none, 1 limited, 2 good, 3 strong) intended to guide pairings that reduce non-identifiability rather than to rank instruments globally. The depth bands are grounded by typical sampling depths: ToF-SIMS is highly surface sensitive and often samples roughly the upper 1–2 nm (Graham *et al*., 2023). XPS is typically surface sensitive within about 0–10 nm (Stevie, 2020; Thermo Fisher, 2025; HarwellXPS, 2019). HAXPES extends probing depth to tens of nanometers, commonly cited up to about 30 nm for buried layers (Risterucci *et al*., 2014; ACS, 2025). Time resolution anchors for structural kinetics are supported by synchrotron in situ GISAXS demonstrations at 200 ms temporal resolution (Saxena *et al*., 2020; Balazs *et al*., 2020).

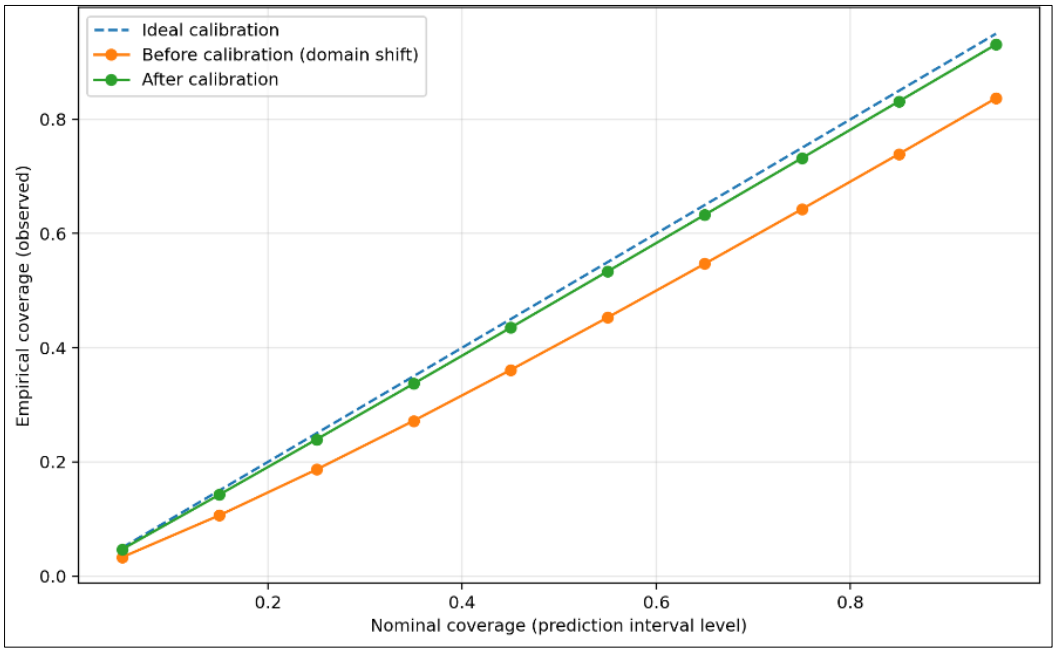

Figure 7: Reliability diagram for uncertainty under domain shift

Figure 8. Reliability diagram showing how uncertainty estimates can become miscalibrated under domain shift and how calibration moves predicted uncertainty toward the ideal diagonal. The plot compares

nominal coverage of prediction intervals to empirical observed coverage. Under domain shift, models often become overconfident or underconfident, meaning the reported uncertainty no longer corresponds to actual error frequencies. Reliability diagrams are a standard diagnostic for uncertainty calibration, and recent UQ literature emphasizes that average calibration alone is insufficient and conditional calibration (adaptivity) matters in practice (Pernot, 2023).

8. Validation, Benchmarking, and End-to-End Case Studies + Outlook

Benchmarking is the place where "design grammar" either becomes engineering knowledge or collapses into non-comparable claims. Across functional-matter domains, most apparent breakthroughs fail for the same reasons: the baseline is not matched, the normalization silently changes, uncertainty is not reported, durability is measured under different stressors, or the reported performance cannot transfer across labs. This is why validation must be treated as a first-class grammar step, not as the last paragraph of a paper. Interlaboratory studies in batteries and impedance metrology show that even when materials are held constant, setup, calibration, temperature control, and assembly parameters can drive large variability in measured performance (Puls *et al*., 2024; Kasper *et al*., 2022).

A practical design-grammar view is to define an "improvement" only when it survives a benchmark truth table: a claim counts only if (i) it beats a matched baseline under the same boundary conditions, (ii) it is normalized in a comparable way, (iii) uncertainty and repeatability are reported, and (iv) durability and validation targets are met. For example, lithium-metal anodes may show short segments of high coulombic efficiency, but long-horizon deployment requires consistently extreme CE, with analysis pointing to >99.9% as challenging and practical requirements pushing toward even higher consistency (Hobold *et al*., 2021; Sun *et al.,* 2025).

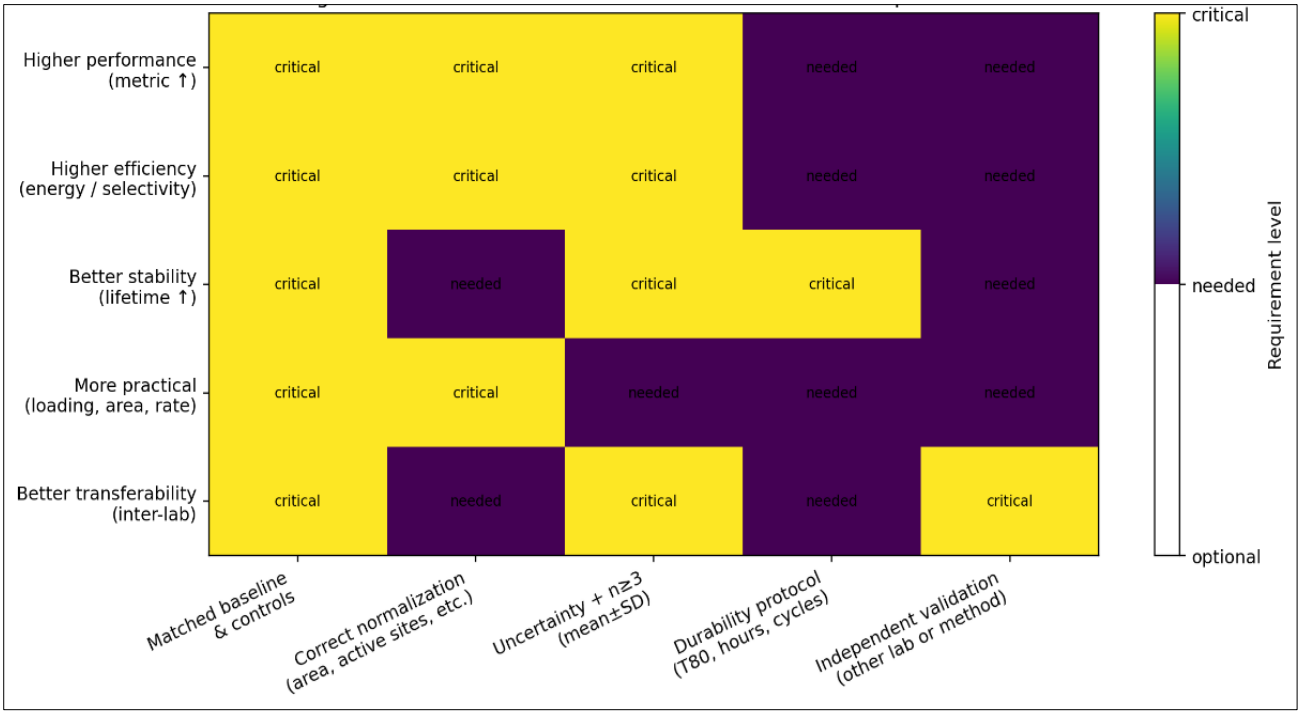

Figure 8: Benchmark truth table for what counts as an improvement

A compact decision matrix that operationalizes benchmarking. Rows represent improvement claim types, columns represent conditions that must be satisfied for the claim to count. "Critical" indicates non-negotiable requirements for fair comparison, "needed" indicates requirements strongly recommended for claim credibility, and "optional" indicates items that improve interpretability but are not always required. The logic aligns with interlaboratory evidence that test setup and calibration can dominate outcomes (Kasper *et al*., 2022; Puls *et al*., 2024).

Fair Benchmarking in Practice: Baselines, Normalization, and Uncertainty

A matched baseline is not "the best number from the literature." It is the best-performing or most-used reference measured in the same hardware and conditions, ideally in the same lab session and preferably with shared materials. In all-solid-state batteries, round-robin and reproducibility work shows that cell assembly details, stack pressure, and test configuration can create large spread across labs, so baseline matching must include the full cell build and test stack (Puls *et al*., 2024).

Normalization must be explicit because it defines what "better" means. In CO2 electroreduction, reporting only current density without product analysis is incomplete; Faradaic efficiency is essential and must be measured and reported carefully to avoid systematic misestimation (Clark *et al*., 2018; Kempler *et al*., 2023). In photovoltaics, measurement standards exist precisely because "efficiency" depends on spectral mismatch, stabilization behavior, and uncertainty control; IEC 60904-1 emphasizes procedures to minimize uncertainty in I–V measurements (IEC, 2020).

Uncertainty and repeatability are not optional when the community is deciding whether a design rule is real. Round-robin impedance studies show that calibration and systematic errors can be comparable to or larger than the performance deltas that papers sometimes claim as breakthroughs (Kasper *et al*., 2022). The minimum credible practice is replicates (commonly $n \geq 3$), reporting mean ± standard deviation, and reporting key sources of measurement uncertainty (temperature stability, fixture resistance, reference calibration, and drift).

Inter-Lab Transfer: The Gatekeeper for "Design Rules"

Inter-lab transfer should be treated as the highest level of validation because it tests whether the grammar generalizes beyond one instrument stack. The most direct mechanism is a round-robin format: shared materials, agreed protocols, and shared reporting templates. This is now common in batteries and measurement standards efforts (Puls *et al*., 2024; VAMAS, 2025). A grammar-ready benchmark report should include not only performance values but also a full "metadata spine" that makes reproduction feasible.

Case A: Solid-State Lithium-Metal Cell under Practical Constraints

Benchmark gate: high areal capacity and energy density targets force thin lithium, high CE, and stable cycling. Techno-economic analysis uses an areal capacity example of 5.4 mAh cm−2 in solid-state architectures and links required CE to capacity retention targets over long cycling (Burton *et al*., 2025). Dominant steps: interfaces/interphases and validation (Figure 10). Validation: reproducibility across labs and explicit reporting of assembly parameters, motivated by interlaboratory variability evidence (Puls *et al*., 2024).

Case B: CO2 Electrolysis at Industrial Current Density

Benchmark gate: cost-competitive CO2 electrolysis is commonly framed around current density exceeding 200 mA cm−2, high selectivity, low overpotential, and long-term operation on the order of thousands of hours, with explicit discussion of these thresholds in high-current-density CO2ER literature (Lin *et al*., 2022; Monteiro *et al*., 2021). Dominant steps: operando characterization, interface control, and validation. Validation: standardized product analysis and reporting guidance to prevent FE overestimation and enable cross-lab comparability (Clark *et al*., 2018; Kempler *et al*., 2023).

Case C: Perovskite Photovoltaics with Stability as the Benchmark

Benchmark gate: stabilized performance and stability under defined stressors, not only a single fast scan. A broad community consensus statement recommends stability assessment and reporting procedures for perovskite PV based on ISOS protocols, including additional procedures for perovskite-specific behavior such as reversible degradation and ion redistribution (Khenkin *et al*., 2020). Dominant steps: characterization and validation, with standardized measurement protocols (IEC, 2020).

Case D: Interface-Engineered Cathode with Coating-Controlled Degradation

Benchmark gate: same active material loading and test window, demonstrate reduced impedance growth and improved retention while controlling for measurement artifacts. Round-robin impedance and battery reproducibility work supports treating calibration and protocol as part of the design, not an afterthought (Kasper *et al*., 2022; Puls *et al.*, 2024).

Case E: Hierarchical Porous Support for Transport-Limited Performance

Benchmark gate: improved performance must persist after normalization by geometric area, catalyst mass, and if possible accessible surface area, while demonstrating that gains are not purely mass-transport artifacts. Gas-involving electrochemistry benchmarking literature highlights how transport, cell design, and reporting choices can dominate apparent activity (Oshchepkov *et al*., 2023; Clark *et al*., 2018).

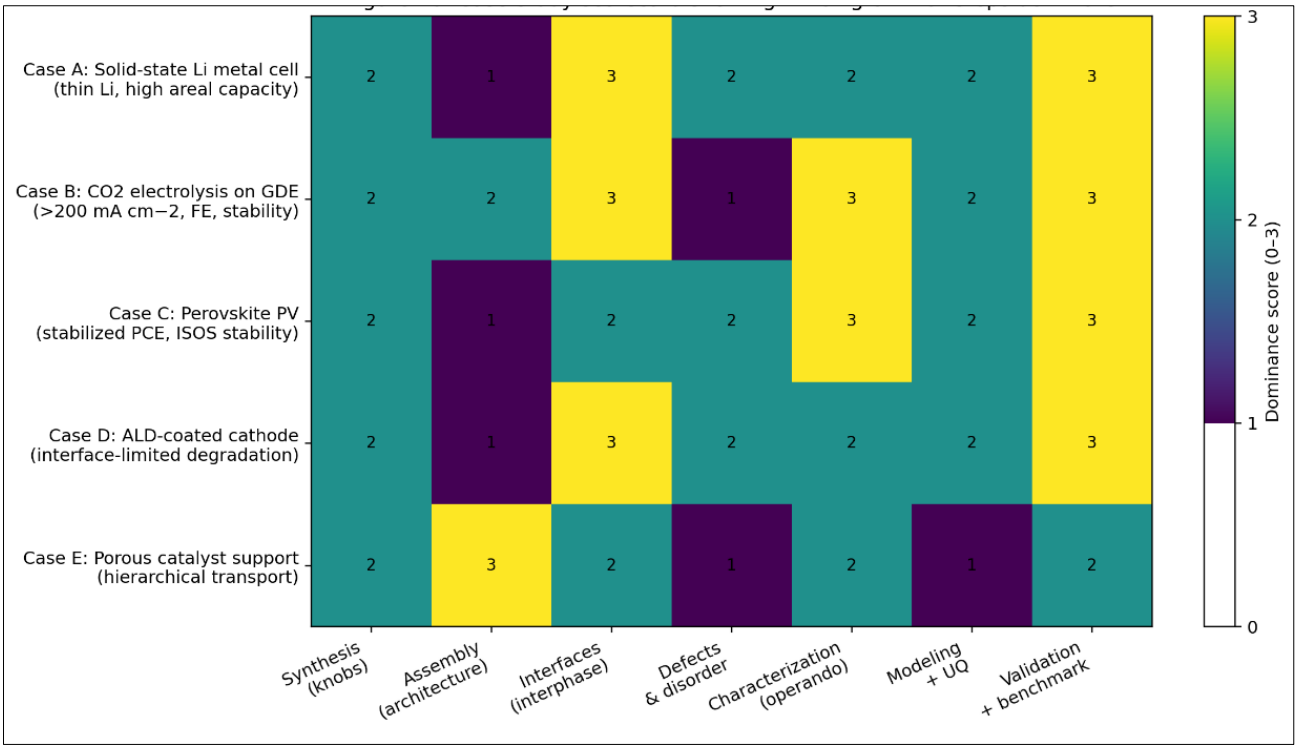

Figure 9: Case-study scorecard showing which grammar steps dominate each case

A dominance score (0–3) heatmap indicating which grammar steps most strongly control outcomes in each case study. The purpose is to tell students where to spend effort first. For example, industrial CO2 electrolysis and solid-state lithium both score high on interfaces, operando characterization, and validation because community guidance and reproducibility studies show those steps often determine whether improvements are real and transferable (Clark *et al*., 2018; Puls *et al*., 2024).

Table 8: Benchmarking protocol checklist and reporting template

What you must report	Minimum benchmarkable value or format	Practical anchor values used in literature	Why it matters
Replicates + statistics	n ≥ 3, report mean ± SD	nLIB = 3 example appears in ASSB benchmarking context (Puls *et al*., 2024)	Prevents single-cell or single-device selection bias
Inter-lab transfer target	At least 2 labs or round-robin format	Reproducibility and round-robin work in batteries and standards bodies (Puls *et al*., 2024; VAMAS, 2025)	Converts “lab effect” into quantified uncertainty
PV standard test conditions	State STC and method, include uncertainty	IEC 60904-1 measurement uncertainty focus (IEC, 2020)	Makes PCE comparable and traceable
Perovskite stability protocol	Use ISOS-based reporting, include stressors	ISOS-based consensus for PSC stability (Khenkin *et al*., 2020)	Prevents uncomparable stability claims
CO2ER industrial relevance gate	Report j, FE, cell area, runtime	j > 200 mA cm−2 and long duration targets discussed for cost-competitive CO2ER (Lin *et al*., 2022); 10 cm2 GDE example in high-rate work (Monteiro *et al*., 2021)	Ensures relevance beyond low-current screening
Faradaic efficiency reliability	Provide product calibration and closure	FE definition and reporting pitfalls emphasized (Kempler *et al*., 2023; Clark *et al*., 2018)	Avoids FE inflation due to missing products or leaks
Li-metal practicality gate	Report areal capacity and CE definition	CE challenges and need for extremely high CE discussed (Hobold *et al*., 2021; Sun *et al*., 2025)	CE differences of 0.1% can dominate lifetime

What you must report	Minimum benchmarkable value or format	Practical anchor values used in literature	Why it matters
Solid-state energy density anchor	Provide areal capacity and architecture	Areal capacity example 5.4 mAh cm−2 used in SSB energy-density analysis (Burton *et al*., 2025)	Forces realistic constraints (thin Li, limited excess)
EIS calibration and bandwidth	State frequency range and calibration	50 mHz to 10 kHz in round-robin EIS work, with systematic-error corrections (Kasper *et al*., 2022)	Prevents "fit looks good" but wrong parameters
Data + metadata release	Provide machine-readable metadata	FAIR principles for data reuse (Wilkinson *et al*., 2016)	Enables reuse, reanalysis, and model validation

9. OUTLOOK AND CONCLUSION

Validation is the mechanism that turns cross-scale design grammar into a reusable engineering language. The near-term opportunity is to standardize "benchmark-ready" reporting templates that include uncertainties, normalization, and metadata, plus targeted inter-lab transfer studies for the most failure-prone claims (interfaces, degradation, and operando inference). Community consensus efforts already show the pattern: perovskite PV moved forward once stability testing and reporting were formalized (Khenkin *et al*., 2020), CO2 electroreduction improved comparability once reporting protocols were articulated (Clark *et al*., 2018), and battery research is now quantifying interlaboratory variability directly (Puls *et al*., 2024; Kasper *et al*., 2022).

The longer-term direction is a shared benchmarking infrastructure: reference materials, open round-robin datasets, and digital benchmark ledgers that are FAIR by construction (Wilkinson *et al*., 2016). In that world, the design grammar becomes measurable: each grammar step earns credibility when it produces improvements that survive baseline matching, correct normalization, uncertainty quantification, durability, and inter-lab validation.

REFERENCES

- Akhter, S., Samanta, A., & Shishodia, P. (2021). Silica aerogels: Synthesis, properties and applications. *Journal of Porous Materials, 28*, 1381–1400. doi:10.1007/s10934-020-00980-8
- Albert, J. N. L., & Epps, T. H. (2010). Self-assembly of block copolymer thin films. *Materials Today, 13*(6), 24–33. doi:10.1016/S1369-7021(10)70057-2
- Baer, D. R., Artyushkova, K., Cohen, H., Easton, C. D., Engelhard, M., Gengenbach, T. R., Greczynski, G., Mack, P., Morgan, D. J., & Roberts, A. (2020). XPS guide: Charge neutralization and binding energy referencing for insulating samples. *Journal of Vacuum Science & Technology A: Vacuum, Surfaces, and Films, 38*(3), 031204. https://doi.org/10.1116/6.0000057
- Bard, A. J., & Faulkner, L. R. (2001). Electrochemical methods: Fundamentals and applications (2nd ed.). Wiley.
- Bauhofer, W., & Kovacs, J. Z. (2009). A review and analysis of electrical percolation in carbon nanotube polymer composites. *Composites Science and Technology, 69*(10), 1486–1498. doi:10.1016/j.compscitech.2008.06.018
- Billinge, S. J. L. (2019). The rise of the X-ray atomic pair distribution function method: A series of fortunate events. Philosophical Transactions of the Royal Society A: Mathematical, Physical and Engineering Sciences, 377, 20180413. https://doi.org/10.1098/rsta.2018.0413
- Binnig, G., Quate, C. F., & Gerber, C. (1986). Atomic force microscope. Physical Review Letters, 56(9), 930–933. https://doi.org/10.1103/PhysRevLett.56.930
- Bolt, R. R. A., Leitch, J. A., Jones, A. C., Nicholson, W. I., & Browne, D. L. (2022). Continuous flow mechanochemistry: Reactive extrusion as an enabling technology in organic synthesis. *Chemical Society Reviews, 51*(11), 4243–4260. doi:10.1039/D1CS00657F
- Bormashenko, E. (2016). Physics of solid-liquid interfaces: From the Young equation to the superhydrophobicity. Low Temperature Physics, 42(8), 622-635.
- Boukhouiete, M., Eshwekin, A., Tighilt, H., & Benayache, S. (2021). Effect of current density on the microstructure and morphology of the electrodeposited nickel coatings. *Turkish Journal of Chemistry, 45*(5), 1329–1339. doi:10.3906/kim-2101-12
- Burdyny, T. E., Sassenburg, M., de Rooij, R., Nessbit, N., Kas, R., Chandrashekar, S., Firet, N. J., Yang, K., Liu, K., Blommaert, M. A., Kolen, M., Ripepi, D., & Smith, W. A. (2022). Characterizing CO_2 reduction catalysts on gas diffusion electrodes: Comparing activity, selectivity, and stability of transition metal catalysts. *ACS Applied Energy Materials, 5*(5), 5983–5994. https://doi.org/10.1021/acsaem.2c00160
- Burton, M., Narayanan, S., Jagger, B., Olbrich, L. F., Dhir, S., Shibata, M., et al. (2025). Techno-economic assessment of thin lithium metal anodes for solid-state batteries. *Nature Energy, 10*(1), 135–147. https://doi.org/10.1038/s41560-024-01676-7
- Celina, M. (2019). Overview of accelerated aging and polymer degradation kinetics: Non-Arrhenius behaviour and other complexities. Polymer Degradation and Stability, 172, 109056. https://doi.org/10.1016/j.polymdegradstab.2019.109056

- Clark, E. L., Resasco, J., Landers, A. T., Lin, J. C., Chung, L.-T., Walton, A., Hahn, C., Jaramillo, T. F., & Bell, A. T. (2018). Standards and protocols for data acquisition and reporting for studies of the electrochemical reduction of carbon dioxide. *ACS Catalysis, 8*(7), 6560–6570. https://doi.org/10.1021/acscatal.8b01340
- Crawford, D. E., James, S. L., & McNally, T. (2018). Use of batch mixing to investigate the continuous solvent-free mechanical synthesis of OLED materials by twin-screw extrusion (TSE). *ACS Sustainable Chemistry & Engineering, 6*(1), 193–201. doi:10.1021/acssuschemeng.7b02202
- du Plessis, A., Broeckhoven, C., Guelpa, A., & le Roux, S. G. (2017). Laboratory x-ray micro-computed tomography: A user guideline for biological samples. *GigaScience, 6*(6), 1–11. https://doi.org/10.1093/gigascience/gix027
- Graham, D. J., & Gamble, L. J. (2023). Back to the basics of time-of-flight secondary ion mass spectrometry of bio-related samples. I. Instrumentation and data collection. *Biointerphases, 18*(2), 021201. https://doi.org/10.1116/6.0002477
- Graham, D. J., Gamble, L. J., Wagner, M. S., Castner, D. G., & Gilmore, I. S. (2023). Back to the basics of time-of-flight secondary ion mass spectrometry of bio-related samples. I. Instrumentation and data collection. Biointerphases, 18(2), 021201. https://doi.org/10.1116/6.0002477
- Graham, D. J., Gamble, L. J., Wagner, M. S., Castner, D. G., & Gilmore, I. S. (2023). Back to the basics of time-of-flight secondary ion mass spectrometry data analysis of bio-related samples. II. Data processing and display. Biointerphases, 18(3), 031201. https://doi.org/10.1116/6.0002633
- Graham, D. J., Wagner, M. S., Castner, D. G., & Gilmore, I. S. (2023a). Tutorial: Time-of-flight secondary ion mass spectrometry (ToF-SIMS) instrumentation, principles and considerations. Biointerphases, 18(2), 020801. https://doi.org/10.1116/6.0002552
- Graham, D. J., Wagner, M. S., Castner, D. G., & Gilmore, I. S. (2023b). Tutorial: Time-of-flight secondary ion mass spectrometry (ToF-SIMS) data collection, analysis, and reporting. Biointerphases, 18(2), 021001. https://doi.org/10.1116/6.0002461
- Hamzaoui, R., & Bouchenafa, O. (2020). Equivalent cement clinker obtained by indirect mechanosynthesis process. *Materials, 13*(21), 5045. doi:10.3390/ma13215045
- Hobold, G. M., Kim, K.-H., & Gallant, B. M. (2023). Beneficial vs. inhibiting passivation by the native lithium solid electrolyte interphase revealed by electrochemical Li+ exchange. Energy & Environmental Science, 16, 2247. https://doi.org/10.1039/D2EE04203G
- Hobold, G. M., Lopez, J., Guo, R., Minafra, N., Banerjee, A., Meng, Y. S., Shao-Horn, Y., & Gallant, B. M. (2021). Moving beyond 99.9% Coulombic efficiency for lithium anodes in liquid electrolytes. *Nature Energy, 6*(10), 951–960. https://doi.org/10.1038/s41560-021-00910-w
- International Electrotechnical Commission. (2020). *IEC 60904-1:2020 Photovoltaic devices Part 1: Measurement of photovoltaic current-voltage characteristics*. Geneva, Switzerland.
- International Union of Pure and Applied Chemistry. (2025). *Kinetic control* (IUPAC Gold Book, Version 5.0.0). doi:10.1351/goldbook.K03398
- International Union of Pure and Applied Chemistry. (2025). *Thermodynamic control* (IUPAC Gold Book, Version 5.0.0). doi:10.1351/goldbook.T06316
- Jagger, B., & Pasta, M. (2023). Solid electrolyte interphases in lithium metal batteries. Joule, 7, 2228-2244. https://doi.org/10.1016/j.joule.2023.08.007
- Jeong, J. W., Park, W. I., Kim, M. J., Ross, C. A., & Jung, Y. S. (2013). Self-assembled nanostructures in block copolymer thin films: From morphologies to functionalities. *Materials Today, 16*(12), 468–476. doi:10.1016/j.mattod.2013.11.008
- Johnson, R. W., Hultqvist, A., & Bent, S. F. (2014). A brief review of atomic layer deposition: From fundamentals to applications. Materials Today, 17(5), 236–246. https://doi.org/10.1016/j.mattod.2014.04.026
- Johnson, R. W., Hultqvist, A., & Bent, S. F. (2014). A brief review of atomic layer deposition: From fundamentals to applications. *Materials Today, 17*(5), 236–246. doi:10.1016/j.mattod.2014.04.026
- Josephson, D. P., Miller, M., & Stein, A. (2014). Inverse opal SiO2 photonic crystals as structurally-colored pigments with additive primary colors. *Zeitschrift für Anorganische und Allgemeine Chemie, 640*(3–4), 655–662. doi:10.1002/zaac.201300578
- Kasper, M., Leike, A., Al-Zubaidi R-Smith, N., Papachristou, A., & Kienberger, F. (2022). Electrochemical impedance spectroscopy error analysis and round robin on dummy cells and lithium-ion-batteries. *Journal of Power Sources, 536*, 231407. https://doi.org/10.1016/j.jpowsour.2022.231407
- Kempler, P. A., & Nielander, A. C. (2023). Reliable reporting of Faradaic efficiencies for electrocatalysis research. *Nature Communications, 14*(1), 1158. https://doi.org/10.1038/s41467-023-36880-8
- Kennedy, M. C., & O'Hagan, A. (2001). Bayesian calibration of computer models. Journal of the Royal Statistical Society: Series B (Statistical Methodology), 63(3), 425-464. https://doi.org/10.1111/1467-9868.00294
- Khenkin, M. V., Katz, E. A., Abate, A., Bardizza, G., Berry, J. J., Brabec, C., et al. (2020). Consensus statement for stability assessment and reporting for perovskite photovoltaics based on ISOS procedures. *Nature Energy, 5*, 35–49. https://doi.org/10.1038/s41560-019-0529-5
- LaMer, V. K., & Dinegar, R. H. (1950). Theory, production and mechanism of formation of monodispersed hydrosols. *Journal of the American Chemical Society, 72*(11), 4847–4854. doi:10.1021/ja01167a001
- Le Saux, V., Le Gac, P.-Y., Marco, Y., & Calloch, S. (2014). Limits in the validity of Arrhenius predictions for field ageing of a silica filled polychloroprene in a marine environment. Polymer Degradation and

Stability, 99, 254-261. https://doi.org/10.1016/j.polymdegradstab.2013.10.027

- Lebrun, D. M., Niklasson, G. A., & Österlund, L. (2014). Fabrication of photonic opal structures on different support materials by convective evaporation. *Journal of Physics: Conference Series, 559*(1), 012007. doi:10.1088/1742-6596/559/1/012007
- Liu, J., & Cao, C. (2016). Capillary pressure induced cracks in drying nanocrystal films. *Scientific Reports, 6*, 23907. doi:10.1038/srep23907
- Liu, Y., Wang, C., Liu, J., Shi, X., Huang, Y., Cheng, Q., … Lu, W. (2026). A multimodal dataset of causal mechanisms in materials science literature. Scientific Data. Advance online publication (Published January 16, 2026). https://doi.org/10.1038/s41597-026-06598-5
- Lou, S., Zhang, F., Fu, C., Chen, M., Ma, Y., Yin, G., & Wang, J. (2021). Interface issues and challenges in all-solid-state batteries: Lithium, sodium, and beyond. Advanced Materials, 33, 2000721. https://doi.org/10.1002/adma.202000721
- Maljuric, S., Jud, W., Kappe, C. O., & Cantillo, D. (2020). Translating batch electrochemistry to single-pass continuous flow conditions: An organic chemist's guide. *Journal of Flow Chemistry, 10*, 181–190. doi:10.1007/s41981-019-00050-z
- Malmgren, S., Ciosek, K., Lindblad, R., Plogmaker, S., Kühn, J., Rensmo, H., Edström, K., & Hahlin, M. (2013). Consequences of air exposure on the lithiated graphite SEI. Electrochimica Acta. https://doi.org/10.1016/j.electacta.2013.04.118
- Malmgren, S., Ciosek, K., Lindblad, R., Plogmaker, S., Kühn, J., Rensmo, H., Edström, K., & Hahlin, M. (2013). Consequences of air exposure on the lithiated graphite SEI. Electrochimica Acta. https://doi.org/10.1016/j.electacta.2013.04.118
- Maxwell, A. S., Broughton, W. R., Dean, G. D., & Sims, G. D. (2005). Review of accelerated ageing methods and lifetime prediction techniques for polymeric materials (NPL Report DEPC-MPR 016). National Physical Laboratory.
- Mayeshiba, T. T., & Morgan, D. (2016). Factors controlling oxygen migration barriers in perovskites. *Solid State Ionics, 296*, 71–77. https://doi.org/10.1016/j.ssi.2016.09.007
- Mingard, K. P., Quested, P. N., & Peck, M. D. (2012). Determination of grain size by EBSD: Report on a round robin measurement of equiaxed titanium (NPL Report MAT 56). National Physical Laboratory.
- National Research Council. (2008). Integrated computational materials engineering: A transformational discipline for improved competitiveness and national security. The National Academies Press. https://doi.org/10.17226/12199
- National Science and Technology Council. (2011). Materials genome initiative for global competitiveness. Executive Office of the President. https://www.mgi.gov/sites/mgi/files/materials_genome_initiative-final.pdf
- Noël, T., Cao, Y., & Laudadio, G. (2019). The fundamentals behind the use of flow reactors in electrochemistry. *Accounts of Chemical Research, 52*(10), 2858–2869. doi:10.1021/acs.accounts.9b00412
- Oshchepkov, A. G., Artyushkova, K., & Arey, B. W. (2023). Critical aspects in the reliable assessment of the activity data in electrocatalysis and related electrochemical processes. *Current Opinion in Electrochemistry, 39*, 101266. https://doi.org/10.1016/j.coelec.2023.101266
- Oviroh, P. O., Akbarzadeh, R., Pan, D., Coetzee, R. A. M., & Jen, T.-C. (2019). New development of atomic layer deposition: Processes, methods and applications. *Science and Technology of Advanced Materials, 20*(1), 465–496. doi:10.1080/14686996.2019.1599694
- Plutschack, M. B., Pieber, B., Gilmore, K., & Seeberger, P. H. (2017). The Hitchhiker's Guide to Flow Chemistry. *Chemical Reviews, 117*(18), 11796–11893. doi:10.1021/acs.chemrev.7b00183
- Pribe, J. D., Richter, B., Leser, P. E., Yeratapally, S. R., Weber, G. R., Kitahara, A. R., & Glaessgen, E. H. (2023). A process-structure-property simulation framework for quantifying uncertainty in additive manufacturing: Application to fatigue in Ti-6Al-4V. Integrating Materials and Manufacturing Innovation, 12, 231–250. https://doi.org/10.1007/s40192-023-00303-9
- Puls, S., Nazmutdinova, E., Kalyk, F., Woolley, H. M., Cheng, Z., Gautam, A., et al. (2024). Benchmarking the reproducibility of all-solid-state battery cell performance. *Nature Energy, 9*(10), 1310–1320. https://doi.org/10.1038/s41560-024-01634-3
- Roy, C. J., & Oberkampf, W. L. (2011). A comprehensive framework for verification, validation, and uncertainty quantification in scientific computing. Computer Methods in Applied Mechanics and Engineering, 200(25-28), 2131-2144. https://doi.org/10.1016/j.cma.2011.03.016
- Santhanagopalan, D., Qian, D., McGilvray, T., Wang, Z., Wang, Y., Leung, K., & Meng, Y. S. (2014). Interface limited lithium transport in solid-state batteries. The Journal of Physical Chemistry Letters, 5(17), 2983-2990. https://doi.org/10.1021/jz402467x
- Saxena, V., & Portale, G. (2020). Contribution of ex-situ and in-situ X-ray grazing incidence scattering techniques to the understanding of quantum dot self-assembly: A review. *Nanomaterials, 10*(11), 2240. https://doi.org/10.3390/nano10112240
- Scotti, K. L., & Dunand, D. C. (2018). Freeze casting: A review of processing, microstructure and properties via the open data repository, FreezeCasting.net. *Progress in Materials Science, 94*, 243–305. doi:10.1016/j.pmatsci.2018.01.001
- Seah, M. P., & Dench, W. A. (1979). Quantitative electron spectroscopy of surfaces: A standard data base for electron inelastic mean free paths in solids. *Surface and Interface Analysis, 1*(1), 2–11. https://doi.org/10.1002/sia.740010103
- She, X., Zhang, Y., Koper, M. T. M., & Smith, W. A. (2022). Challenges and opportunities in electrocatalytic CO_2 reduction to chemicals and fuels. *Angewandte Chemie International Edition*. https://doi.org/10.1002/anie.202211396

- Stevie, F. A., & Donley, C. L. (2020). Introduction to X-ray photoelectron spectroscopy. Journal of Vacuum Science & Technology A: Vacuum, Surfaces, and Films, 38(6), 063204. https://doi.org/10.1116/6.0000412
- Sukweenadhi, J., Setiawan, K. I., Avanti, C., Kartini, K., Rupa, E. J., & Yang, D.-C. (2021). Scale-up of green synthesis and characterization of silver nanoparticles using ethanol extract of *Plantago major* L. leaf and its antibacterial potential. *South African Journal of Chemical Engineering*. doi:10.1016/j.sajce.2021.06.008
- Suryanarayana, C. (2001). Mechanical alloying and milling. *Progress in Materials Science, 46*(1–2), 1–184. doi:10.1016/S0079-6425(99)00010-9
- Terban, M. W., & Billinge, S. J. L. (2021). Structural analysis of molecular materials using the pair distribution function. Chemical Reviews. https://doi.org/10.1021/acs.chemrev.1c00237
- Thommes, M., Kaneko, K., Neimark, A. V., Olivier, J. P., Rodriguez-Reinoso, F., Rouquerol, J., & Sing, K. S. W. (2015). Physisorption of gases, with special reference to the evaluation of surface area and pore size distribution (IUPAC Technical Report). *Pure and Applied Chemistry, 87*(9–10), 1051–1069. doi:10.1515/pac-2014-1117
- Ting, J. Y. C., & Barnard, A. S. (2022). Data-driven causal inference of process-structure relationships in nanocatalysis. Current Opinion in Chemical Engineering, 36, 100818. https://doi.org/10.1016/j.coche.2022.100818
- Tobias, A. V., & Wahab, A. (2025). Autonomous 'self-driving' laboratories: A review of technology and policy implications. Royal Society Open Science, 12(7), 250646. https://doi.org/10.1098/rsos.250646
- Tom, G., Schmid, S. P., Baird, S. G., Cao, Y., Darvish, K., Hao, H., Lo, S., Pablo-García, S., Rajaonson, E. M., Skreta, M., Yoshikawa, N., Corapi, S., Akkoc, G. D., Strieth-Kalthoff, F., Seifrid, M., & Aspuru-Guzik, A. (2024). Self-driving laboratories for chemistry and materials science. Chemical Reviews, 124(16), 9633–9732. https://doi.org/10.1021/acs.chemrev.4c00055
- Tuomisto, F., & Makkonen, I. (2013). Defect identification in semiconductors with positron annihilation: Experiment and theory. Reviews of Modern Physics, 85(4), 1583-1631. https://doi.org/10.1103/RevModPhys.85.1583
- Varivoda, D., Dong, R., Omee, S. S., & Hu, J. (2023). Materials property prediction with uncertainty quantification: A benchmark study. Applied Physics Reviews, 10(2), 021409. https://doi.org/10.1063/5.0133528
- Venugopal, V., & Olivetti, E. (2024). MatKG: An autonomously generated knowledge graph in material science. Scientific Data, 11, 217. https://doi.org/10.1038/s41597-024-03039-z
- West, A. R. (2014). *Solid state chemistry and its applications* (2nd ed.). John Wiley & Sons.
- Wexler, R. B., Gautam, G. S., Stechel, E. B., & Carter, E. A. (2021). Factors governing oxygen vacancy formation in oxide perovskites. Journal of the American Chemical Society, 143(33), 13212-13227. https://doi.org/10.1021/jacs.1c05570
- Whitehead, C. B., Özkar, S., & Finke, R. G. (2021). LaMer's 1950 model of particle formation: A review and critical analysis of its classical nucleation and fluctuation theory basis, of competing models and mechanisms for phase-changes and particle formation, and then of its application to silver halide, semiconductor, metal, and metal-oxide nanoparticles. *Materials Advances, 2*, 186–235. doi:10.1039/D0MA00439A
- Wilkinson, M. D., Dumontier, M., Aalbersberg, I. J. J., Appleton, G., Axton, M., Baak, A., … Mons, B. (2016). The FAIR guiding principles for scientific data management and stewardship. Scientific Data, 3, 160018. https://doi.org/10.1038/sdata.2016.18
- Wu, S., Reeve, M., Yoshida, K., & Ghosh, S. (2016). Magnetic alignment of Fe3O4 tethered graphene nanoplatelets in epoxy composites. Polymer, 107, 38–46. doi:10.1016/j.polymer.2016.05.024
- Zang, X., Wang, V. B. E., Lange, M., Capolungo, L., McDowell, D. L., Kumar, M., & Curtin, W. A. (2025). PSP-GEN: Stochastic inversion of the process-structure-property chain in materials design through deep, generative probabilistic modeling. Acta Materialia. https://www.sciencedirect.com/science/article/pii/S1359645424009480
- Zhao, Q., et al. (2021). On the crystallography and reversibility of lithium electrodeposits at ultrahigh capacity. Nature Communications, 12, 6034.